Analyst

ROYAL SOCIETY OF CHEMISTRY

CRITICAL REVIEW

View Article Online
View Journal | View Issue

Cite this: *Analyst*, 2022, **147**, 2895

Microfluidic flow cytometry for blood-based biomarker analysis

Yuxin Zhang, †[a] Ying Zhao,†[b] Tim Cole, [a] Jiahao Zheng,[a] Bayinqiaoge,[a] Jinhong Guo *[c] and Shi-Yang Tang *[a]

Flow cytometry has proven its capability for rapid and quantitative analysis of individual cells and the separation of targeted biological samples from others. The emerging microfluidics technology makes it possible to develop portable microfluidic diagnostic devices for point-of-care testing (POCT) applications. Microfluidic flow cytometry (MFCM), where flow cytometry and microfluidics are combined to achieve similar or even superior functionalities on microfluidic chips, provides a powerful single-cell characterisation and sorting tool for various biological samples. In recent years, researchers have made great progress in the development of the MFCM including focusing, detecting, and sorting subsystems, and its unique capabilities have been demonstrated in various biological applications. Moreover, liquid biopsy using blood can provide various physiological and pathological information. Thus, biomarkers from blood are regarded as meaningful circulating transporters of signal molecules or particles and have great potential to be used as non (or minimally)-invasive diagnostic tools. In this review, we summarise the recent progress of the key subsystems for MFCM and its achievements in blood-based biomarker analysis. Finally, foresight is offered to highlight the research challenges faced by MFCM in expanding into blood-based POCT applications, potentially yielding commercialisation opportunities.

Received 17th February 2022,
Accepted 20th April 2022

DOI: 10.1039/d2an00283c

rsc.li/analyst

1 Introduction

Flow cytometry is a powerful single cell analysis instrument which has been widely utilised for disease diagnostics after its innovation in the late 1960s, as a result of its unique characteristics including accurate cell counting, and high-resolution detecting and sorting.[1] Most conventional flow cytometry is based on fluorescence or impedance methods to achieve cell detection or sorting by pumping fluid containing samples into narrow flow chambers which are designed for related signal generation and acquisition. When samples pass through the flow chambers, corresponding signals are generated and analysed. Researchers are able to characterise the biological and physical information of samples, for example, micro-organisms, viruses, and individual cells with the assistance of flow cytometry. More importantly, flow cytometry can conduct analysis in a non-destructive and high throughput manner.

As illustrated in the left side of Fig. 1, four essential functional systems are typically assembled in modern flow cytometers: modules for sample focusing, detecting, sorting, and data analysing. Usually, a flow cytometry analysis is performed in the following steps to investigate sample properties individually. First, samples are mixed with buffer to create a solution which is then pumped into a detection chamber. The sample tends to suspend in the solution randomly, therefore, a focusing system is used to narrow the sample solution to a core flow for passing through the detecting module. After acquiring related signals from the detection system, the sorting system is activated to allow for the separation and collection of the target cells. Although flow cytometers have become a basic establishment for the bioassays, normally, they are regarded as complex and costly instruments. To acquire signals in multiple dimensions, an optical-based flow cytometer needs to integrate more than one unit of optical detection setup including bulky laser generators, lenses, filters, and photosensors. Thus, most commercial flow cytometers have a high demand in daily maintenance and operation, which hinders their wide applications in different areas and fields such as diagnostics in low-resource settings and point of care (POC) testing.[2]

The last few decades have seen the emergence and growth of microfluidic technology. Microfluidics is the technology of manipulation of fluid in microchannels with dimensions in the range of tens of micrometres, and it has expanded rapidly

[a]*Department of Electronic, Electrical and Systems Engineering, University of Birmingham, Edgbaston, Birmingham, B15 2TT, UK. E-mail: S.Tang@bham.ac.uk*
[b]*National Chengdu Centre of Safety Evaluation of Drugs, West China Hospital of Sichuan University, Chengdu, China*
[c]*The M.O.E. Key Laboratory of Laboratory Medical Diagnostics, The College of Laboratory Medicine, Chongqing Medical University, #1 Yixueyuan Road, Yuzhong District, Chongqing, 400016, China. E-mail: guojinghong@cqmu.edu.cn*
†These authors contributed equally to this work.

into the field of cell biology and many other fields.[1,3–5] To overcome the drawbacks of conventional flow cytometers, scientists and engineers applied microfluidic technologies to flow cytometry, resulting in microfluidic flow cytometry. In a microfluidic flow cytometer (MFCM), samples can be confined in micrometre-sized chambers and channels that are compatible with their intrinsic volume, thus significantly reducing the amount of dilution or buffer solution required. MFCM also enables the integration of multiple liquid manipulation processes required in multi-step analytic processes, such as pumping, sampling, dispensing, and sequential loading and washing. The chip format also provides more versatile detecting and sorting methods, for example, multiple detection units can be integrated, and the sorting approach can be varied based on the target sample. These lab-on-a-chip methods have become a potential solution for compact, rapid, and accurate POC diagnostics in underdeveloped settings.[3,6–8]

A schematic illustration of a microfluidic flow cytometer is shown in Fig. 1 (right side). By applying precise pumping, a sample can be manipulated in the microchannels as desired. The small size of microfluidic chips means a reduced amount of sample and reagent is normally needed for MFCMs. Moreover, the disposable microchip significantly reduces the cost and avoids cross-contamination. In addition, the integrated detection units can be optimised and miniaturised according to the microchip. Therefore, a MFCM usually has a smaller size. With the rapid development of electronics and computer science, data processing has become easier to be miniaturised and integrated into the systems. However, compared to conventional flow cytometers, MFCMs show their own disadvantages. For example, a lower flow rate for bio sample transportation exists in many microfluidic applications. Researchers and engineers are still seeking for solutions to integrate and simplify functional subsystems on microchips.

Biomarkers are commonly found in bodily fluids or tissues and can reflect cellular and molecular variations. As a result, it is instrumental for clinical diagnostic and therapeutic applications that disease-related biomarkers can be detected and quantified.[7] Circulating nucleic acids, metabolites, single cells, and viruses existing in living tissues, cells, or bodily fluids constitute all varieties of human biomarkers. Monitoring of conversions, increasing, or decreasing of these biomarkers can be regarded as clinical criteria to prove disease or even forecast disease developments.[9–11] Therefore, biomarkers play a significant role in POC diagnostics, medicine monitoring, and therapeutical arrangement.

Blood, as the most important bodily fluid, is capable of indicating a wide range of physiological and pathological properties. Also, various advantages make blood one of the most common choices of liquid biopsy, for example, it is a well-defined material and it is accessible depending on the testing requirements.[8] Therefore, blood-based biomarkers are utilised as signal transporters in the circulating system, showing various physiological and pathological conditions and might be applied in non-invasive diagnostic methods. Common biomarkers in blood and diseases that can be diagnosed based on these biomarkers are listed in Table 1.[7,12,13]

Yuxin Zhang

Yuxin Zhang received his B.Eng (1st class honours) in Mechatronics Engineering from the Beijing Jiaotong University, China and the University of Wollongong, Australia in 2019. He is currently a PhD student at the University of Birmingham, UK. His research interest is microfluidics flow cytometry and modular microfluidics.

Jinhong Guo

Dr Jinhong Guo received the bachelor's degree in electronic engineering from the University of Electronic Science and Technology of China, Chengdu, China in 2010 and PhD degree in biomedical engineering from the Nanyang Technological University in 2014. Currently, he is a full professor in Shanghai Jiao Tong University, China and executive Dean of Chongqing Medical University, China. After his doctoral studies, he was a postdoctoral fellow in the Pillar of Engineering Design at MIT-SUTD Singapore from 2014 to 2015. He then worked as a Visiting Professor in the School of Mechanical Engineering at University of Michigan, Ann Arbor from January 2016 to July 2016. His current research focuses on Electrochemical Sensor and lab-on-a-chip devices for Point of Care Test toward clinical use. He is a recipient of the China Sichuan Thousand Talents Plan for Scholars Award (2015) and Chengdu Expert in Science and Technology Award (2015). He has published over 100 journal papers.

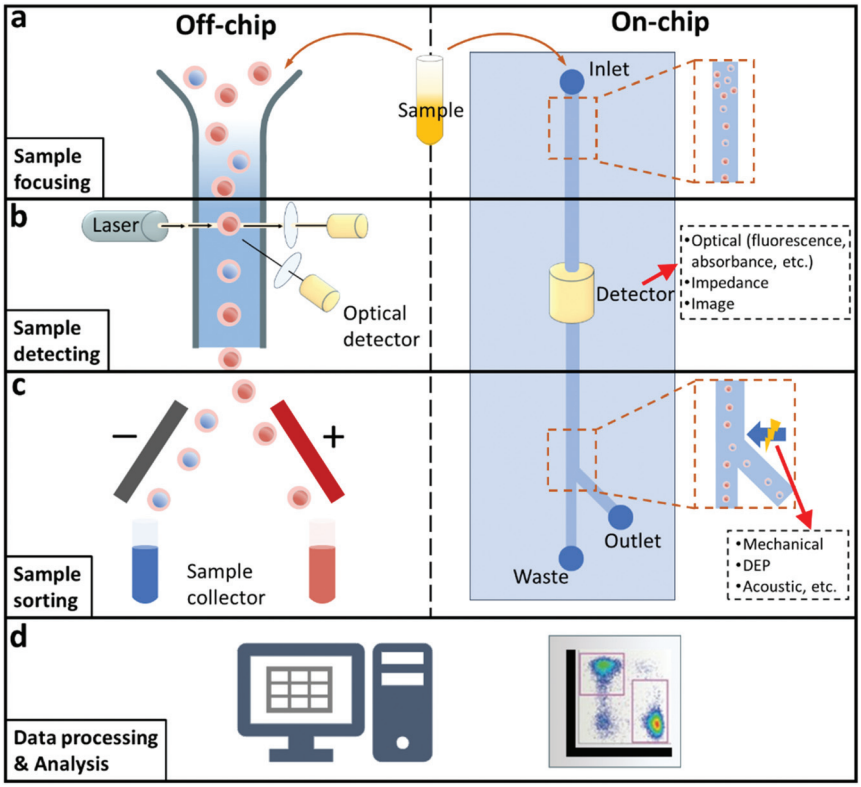

Fig. 1 Schematic illustration of typical off-chip (left side) and on-chip (right side) flow cytometry setup and workflow including (a) Sample focusing. (b) Sample detecting. (c) Sample sorting. (d) Data processing & analysis.

In this review, we seek to examine and summarise the recent major developments of MFCMs for blood-based biomarker analysis. We will outline the key enabling technologies (including sample focusing, detecting, and sorting) and recent advances, as well as discuss challenges and future trends as research progresses towards commercial platforms.

Shi-Yang Tang

Dr Shi-Yang Tang currently is a Lecturer (Assistant Professor) in the Department of Electronic, Electrical and Systems Engineering at the University of Birmingham, UK. He received his BEng (1st class honours) in Electrical Engineering and PhD in Microelectromechanical Systems (MEMS) from the RMIT University, Australia, in 2012 and 2015, respectively. He was the recipient of the Discovery Early Career Researcher Award from the Australian Research Council, and the Vice-Chancellor's Postdoctoral Research Fellow from the University of Wollongong, Australia. Dr Tang's research interests include developing microfluidic platforms for biomedical studies and liquid metal enabled micro-/nanoscale platforms. He has published more than 90 journal papers.

2 Focusing systems for microfluidic flow cytometry

In a typical MFCM, to avoid the simultaneous presence of multiple samples in the detection area, proper strategies need to be applied to narrow down the sample suspension stream. By properly focusing the samples, they can be reordered along the central line without contacting each other and the flow cell wall. Eliminating the instability of the sample velocity *via* proper alignment strategies also ensures the accuracy of acquired signals and the accuracy of the sample sorting process downstream. Therefore, an effective microfluidic focusing system plays a crucial role in a high-performance MFCM. Here, we briefly summarise common strategies adopted for sample focusing, more detailed reviews on this topic can be found elsewhere.[26]

2.1 Hydrodynamic focusing system

Hydrodynamic based focusing systems are the most common technique to narrow sample flow and have been widely used in conventional flow cytometry applications. The emerging MFCMs also take advantage of this technique. By verifying the

Table 1 List of biomarkers in blood

Biomarker category	Sub-categories	Diseases	Ref.
Circulating nucleic acids	• Cell free DNA (cfDNA) • RNA	• Cancer • Viral infection • Hepatitis • AIDS • Bacterial infection • Influenza	14–16
Metabolites	• Prostate-specific antigen	• Prostate cancer	17–19
	• Matrix metalloproteinase	• Endometriosis, breast cancer	
	• β-Galactosidase	• Bacterial infection	
	• Cellobiohydrolase	• Bacterial infection	
	• Glucose oxidase	• Diabetes	
	• Catalase	• Infection, inflammation, cancer	
	• C-reactive protein		
Cells	• Circular tumour cell (CTC)	• Cancer	20–23
	• Bacteria	• Bacterial infection	
	• Fungi	• Nosocomial infection	
Viruses	• Hepatitis viruses • Human immunodeficiency viruses (HIV) • Influenza viruses	• Viral infection • Dengue	24 and 25

microchannel geometries, the focusing performance can be significantly improved and the overall size can be further reduced. Additionally, the simple and straightforward working mechanism makes it possible to easily modify the associated microchannel geometries and achieve mass production at a low cost using standard manufacturing processes such as thermal plastic injection moulding and soft lithography. However, for a planar hydrodynamic focusing technique, the sample core flow can only be limited in the horizontal plane, which hinders its potential to be used in applications with high precision requirements such as image-based detection.

As shown in Fig. 2a, 2D focusing is defined as the horizontal narrowing of samples to the centre plane of a channel, with samples still spread over the microchannel depth. The recent advances and applications of 2D focusing have been comprehensively reviewed in recent publications.[27,28] This focusing method is mainly capable of particle sorting applications despite the fact that particle adsorption to the above and below channel walls might be a problem at times. Recent advances such as image-based flow cytometry require high detection sensitivity, and 3D focusing-horizontal and vertical sample focusing, is necessary.[26] The 2D hydrodynamic focusing is the most commonly used method in MFCM due to its simple fabrication process, simple control requirement, and high throughput. However, the lack of control of particle position in the vertical direction limits the stability of signals.

As shown in Fig. 2b, 3D microfluidic focusing methods limit the core flow both horizontally and vertically, and, therefore, provide more accurate and reliable signals. However, because of the planar fabrication process of microchips, realising on-chip 3D focusing demands more effort than 2D focusing. Normally, multiple-layer microchip designs were used to accomplish 3D hydrodynamic focusing, in which the sample stream is constrained to the centre by sheath flows.[26] Alternatively, as an example, a 3D focusing MFCM using hydrodynamic forces by applying a micro-weir structure design at the bottom of the channel was developed by Fu *et al.*[29] The suggested platform effectively separated microbeads with different diameters (5 μm and 10 μm) in the vertical direction. It was also demonstrated that separating the samples caused their sequential passage through the device's interrogation chamber, which increased the detection process' performance. The same group later employed the Saffman shear lifting force created by a sequence of micro-weirs of gradually decreasing height to focus the sample stream along the centre-line of the microchannel in a 3D focusing sheathless MFCM.[30] The newer design achieved a focusing performance of above 99.5% for microbeads with diameters of 5 and 10 μm. The 3D hydrodynamic focusing method largely improves sensitivity level and holds its advantage of high throughput. However, it requires more complex fabrication process and complicated fluid pumping systems.

2.2 Inertial focusing systems

Cross-stream particle motion is used in inertial focusing methods to concentrate particles into one or multiple streams (Fig. 2d). Different channel designs have been investigated for affecting the inertial focusing results, including straight channels,[31–33] curved channels,[34–36] and type-specific (*e.g.*, groove-structure) channels.[37–41] In a channel flow, samples are affected by both shear gradient and wall effect forces, and sample focusing happens whenever these combined forces are balanced. Particles, cells, viruses, and other items have been counted and sorted using inertial focusing microfluidic cytometers.[42] Oakey *et al.*,[43] for example, built a staged inertial-based microfluidic system with both straight and curved channel designs to restrict particles into a core flow without the use of a sheath flow. The suggested channel's accuracy was found to be comparable to commercial cytometers with hydrodynamic focusing systems. Furthermore, the device's performance was shown to enhance as the flow rate increased, indicating that it has the capability to be used in high-throughput analytical settings. Tang *et al.*[44] demonstrated an impedance-based MFCM with liquid electrodes and an inertial focusing module. The practicality of the suggested cytometer was proved by examining the size distributions of white blood cells (WBCs) and breast tumour cells (MCF-7) in human whole blood samples. Unlike the hydrodynamic focusing, well-designed microchannel structures ensure its advantages in simple fluidic (due to sheathless) control and throughput. However, the specific geometry and requirement on precise flow rate limit its popularisation in MFCMs.

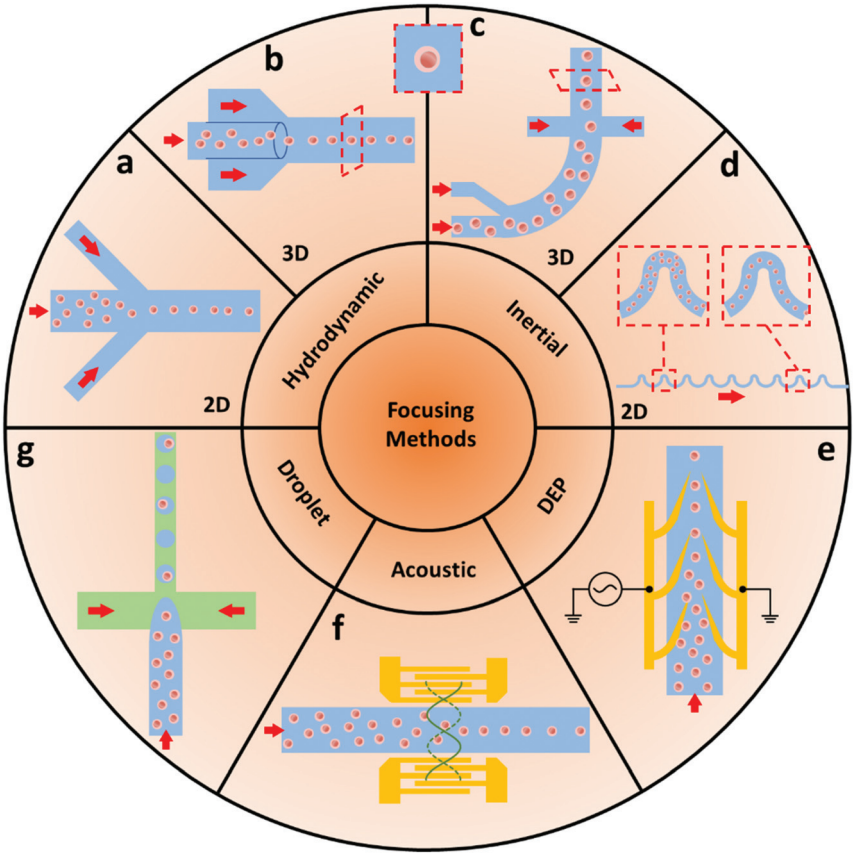

Fig. 2 Schematic of sample focusing methods used in MFCMs. Typical methods are based on (a and b) hydrodynamic, (c and d) inertial, (e) DEP, (f) acoustic, and (g) droplet-based techniques.

2.3 Dielectrophoresis based focusing systems

Dielectrophoresis (DEP) is a commonly used method for manipulating cells, particles, DNAs, viruses, and many other items in microfluidic systems.[45–47] DEP is also widely employed in a range of bio-sensing devices for trapping, patterning, focusing, separating, transporting, and depositing. The DEP force is affected by particle diameter, dielectric characteristics of the particles, and the fluid through which they are conveyed. Furthermore, the DEP force changes as a function of frequency in an alternating current (AC) field. The DEP response may be adjusted from negative (particles are rejected from high-intensity field zones) to positive (particles are drawn to high-intensity field zones) based on the dielectric characteristics of the fluid and particle. The crossover frequency is the frequency where this change happens. Negative DEP forces were typically used in electrode-based DEP 2D focusing techniques.[48] To achieve 3D focusing, combining with other focusing strategies is necessary. For example, Lin *et al.*[49] designed a 3D focusing platform combining hydrodynamic forces and a vertically applied negative DEP force. Polystyrene microbeads (diameters of 10 and 20 μm) and diluted human RBCs were used to illustrate the practicality of the proposed technology. The DEP force increased the consistency of the acquired signal amplitude, which improved the accuracy and consistency of the detection findings. The DEP focusing provides a high level in sensitivity but at the same time sacrifices the throughput. Also, the additional microfabrication process of microelectrodes and the frequency dependent complex control constrain its utilisation in MFCM.

2.4 Acoustic focusing systems

Large forces may be generated on samples in a microfluidic device using acoustic fields. The samples can migrate toward either the pressure nodes or the antinodes as a result of acoustic manipulation, depending on the particle density and deformability, as well as the environment in which they are dispersed, as illustrated in Fig. 2f.[50] Moreover, the particles can be driven to migrate within a microfluidic channel by activating a sequence of interdigital transducers (IDTs) on a piezoelectric material at their resonance frequencies, resulting in a sample movement effect.[51–53]

Numerous approaches for microfluidic manipulation utilising either travelling surface acoustic waves (TSAWs)[54,55] or standing surface acoustic waves (SSAWs)[56,57] have been reported in various studies. Surface acoustic wave (SAW)-based systems offer a large working frequency range (1 MHz–1 GHz, corresponding to acoustic wavelengths of 4–4000 μm on a piezoelectric lithium niobate substrate) with high biocompat-

ibility for microspheres handling.[58] Recent research has revealed that acoustic fields can not only be utilised to transport samples at the microscopic level, but they can also be used to focus samples efficiently. For example, Collins and Ai *et al.*[58–61] applied a group of IDTs to generate narrow acoustic beams with a width of 10–20 μm. Also, a series of hybrid focusing methods combing hydrodynamics and acoustic were developed by Huang's group to enhance the focusing performance and reduce the fabrication process.[62–64]

Acoustic based focusing systems have been successfully applied on MFCM for a wide range of bio samples. Chen *et al.*[65] developed an SSAW-based MFCM wherein the samples were focused by a 3D focusing field formed by twin IDTs and detected using a laser-based fluorescence approach in the downstream detection chamber. At a rate of ~1000 particles per s, the suggested system has a coefficient of variation of less than 10%, according to the result acquired using calibrating beads. With a planar electrode Coulter-type impedance spectrometer, Grenvall *et al.*[66] developed an acoustic focusing microchip enabling sheathless focusing of cells and particles, as well as subsequent separating and counting. The system was applied to analyse single and mixed size particle suspensions, and also diluted whole blood samples. The findings were found to be quite comparable to those found using a standard standalone Coulter counter. The acoustic focusing system can maintain high throughput and sensitivity, but the requirement of specific piezoelectric transducers may introduce more cost and complexity.

2.5 Droplet-based focusing systems

In the past decade, droplet-based microfluidics has emerged as a powerful tool for the encapsulation and manipulation of individual cells in a high-throughput manner within pico-litre microdroplets, which has revolutionised the study of single cell analysis.[4,67,68] For encapsulating single cells, a cell suspension is dispensed into a single droplet in the oil phase (Fig. 2g). Then the generated microdroplets are reinjected into a customised detection chamber of the MFCM. In the following detection system, instead of detecting labelled individual cells, cell-laden microdroplets are targeted. In this case, the focusing step is simplified since the aimed size is enlarged from individual cells to cell-laden microdroplets, where droplets are narrowed within the interrogation flow channel and driven through the detection unit in order. Then the data is acquired, and the desired sample can be sorted along with its droplet compartment in the sorting unit downstream. Instead of acting on individual cells, the droplet-based focusing method provides an alternative approach, which allows the detecting and sorting system to directly target based on the content of the individual droplets. Baret *et al.* built a fluorescence-activated droplet sorting (FADS) system that was designed to sort picolitre-sized microdroplets by DEP. In this work, no focusing model is involved and the aqueous droplets flow through the fluorescence-based detecting system in sequence which finally achieved an accurate sorting result. Water-in-oil microdroplets were pumped into a microchip sorter in which samples were spaced out and separated at a Y-shaped structure. Similarly, to identify the cells with high α-amylase expression, Sjostrom *et al.*[69] employed a FADS platform to screen a yeast library with mutations randomly inserted across the genome by UV-irradiation mutagenesis. Over the process of about 2 h, nearly 3×10^6 microdroplets were sorted at a frequency of 323 samples per second. With the aid of the droplet technique, no conventional focusing module is required. Unlike the conventional on-chip process, Cole *et al.*[70] developed printed droplet microfluidics technology, where individual cells and reagents were encapsulated in microdroplets and then a fluorescence-based droplet sorter actively selected and deposited desired samples on an arrayed format substrate. As a new focusing concept to treat droplets as the target, the aimed size is enlarged from individual sample to sample-laden microdroplets, which allows high sensitivity and throughput. However, the droplet size needs to be precisely controlled actively or passively.

3 Detecting systems for microfluidic flow cytometry

The detection capability of MFCMs is dependent on samples being precisely streamwise positioned such that they are able to pass the interrogation chamber in a single line. Optical scattering-based approaches have typically been used to identify and analyse focused samples[71–80] (Fig. 3a). However, imaging-based detection[81–90] (Fig. 3b) and impedance-based detection[91–98] (Fig. 3c) have become progressively universal in the past decade. We will briefly summarise these techniques in the following sections, full details of them have been reviewed elsewhere.[95,99–101]

3.1 Optical-based detecting systems

Forward scatter (FSC) and side scatter (SSC) signals, as well as at least a few fluorescence colours signals, are always acquired by traditional flow cytometers.[102,103] The FSC and SSC data reveal sample size and internal granularity, whereas the fluorescent data allows immunophenotyping to be used to distinguish between distinct sample types. To realise the miniaturisation of this optical system in MFCMs, recent efforts were made from different perspectives. For example, Fig. 3a shows a typical optical-based detecting module on MFCM. The exciting laser beams were shaped and focused on the sample flow area, and the integrated optical components downstream collected the FSC and SSC information which were detected by photomultiplier tubes (PMTs) with appropriate band pass filters.

3.2 Image-based detecting systems

Image-based analysis detection approaches for MFCMs integrate the high-resolution cell imaging abilities of microscopes with the high-throughput capability of conventional MFCMs. Optical imaging is, without a doubt, the most effective method for visualising live cells with great spatiotemporal resolution. As a result, optical imaging techniques are progressively being

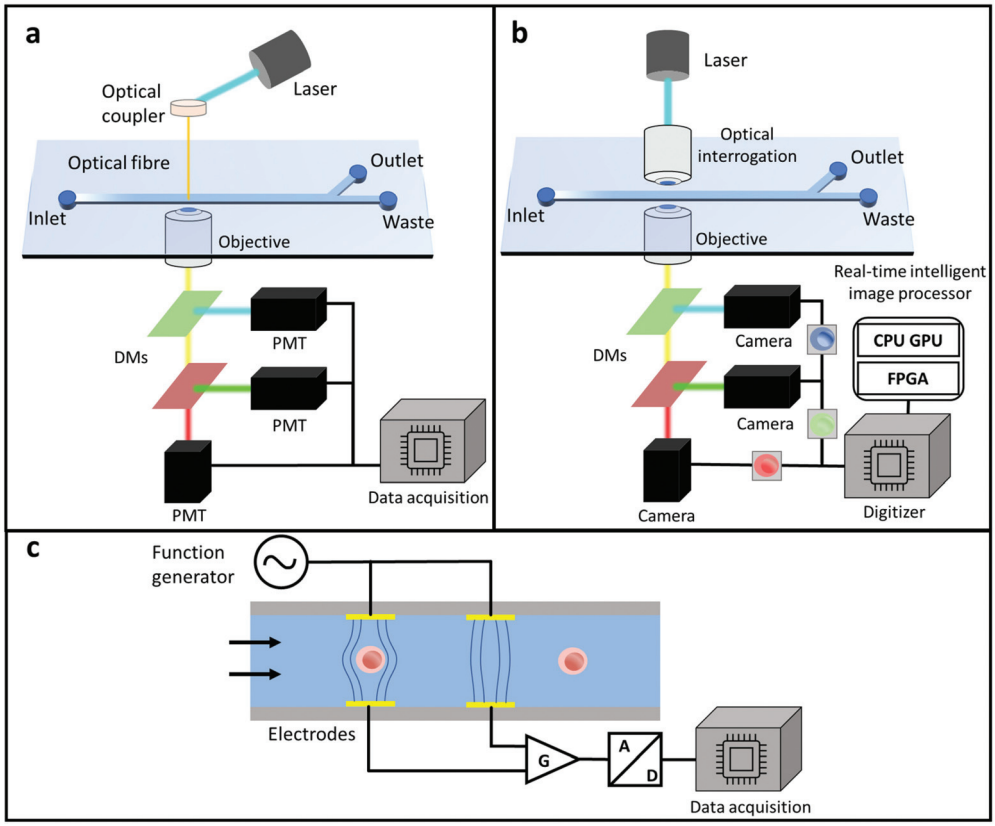

Fig. 3 Schematic of sample detecting system setups in microfluidic flow cytometry. Typical methods are based on (a) optic-based detection, (b) image-based detection, and (c) impedance-based detection.

used in state-of-the-art cellular assay procedures for the categorization of distinct cell types/stages and dissection of their individual cellular activities. Introducing imaging capabilities to MFCMs, however, limits the throughput to ~1000 cells per second, which is significantly less than 100 000 cells per second for gold-standard flow cytometers. Normally, the detecting sensors applied in image-based MFCMs can be divided into two types: (1) camera-based imaging sensors such as charge coupled devices (CCD) and complementary metal–oxide-semiconductor (CMOS) devices;[81,99,104–106] and (2) photodetector-based imaging devices.[107–110] As shown in Fig. 3b, in imaging-based MFCM systems, utilising camera-based devices and a wide-field illumination approach, 2D bio sample imaging could be easily achieved provided that enough photons are detected during a set exposure time. In this case, the dilemma is that of enhancing the image processing speed.

Machine learning (ML), as a winner in processing various image information in recent years, is increasingly bound to microfluidics in the form of intelligent microfluidics thus making detection more automated and intelligent.[83,111,112] Image-based detecting MFCM systems, due to their applicability to ML, especially the presently hottest network-based ML, are gaining more attention from researchers. For example, Heo *et al.*[81] built a convolutional neural network (CNN) image recogniser supported image-based detecting system that analyses images captured from CMOS camera for label-free detection of blood cells. Since this system utilised a multi-target tracking algorithm, all cells in a single image can be analysed simultaneously. Therefore, it offered the possibility to improve throughput and achieve real-time analysis. In addition, Isozaki *et al.*[85] achieved high precision and sensitive detection of cells by acquiring virtual-freezing fluorescence images with a CMOS camera, aided by a 6-layers CNN.

3.3 Impedance-based detection systems

Impedance-based MFCM measures the impedance of a single cell in a detection region and therefore directly reflect the cell's dielectric character.[113] As shown in Fig. 3c, representatively, this setup features microchips where each sample passing by an integrated detection area is examined individually in an electric field. The dielectric characteristics of the cell within will determine the impedance spectrum of the control volume. The cell membrane provides a significant barrier to current flow at low frequencies, and the impedance amplitude predicts the size of a cell. Membrane polarisation is diminished at intermediate frequencies, and impedance analyses provide information regarding membrane characteristics. The membranes are minimally polarised at high frequencies;

therefore, examinations here provide information on intracellular architecture and the cell interior. As a result, analysing the dielectric spectrum in the frequency range from 40 Hz to 1 GHz offers frequency-dependent information on membrane capacitance, cytoplasm conductivity, and cytoplasm permittivity. There are different kinds of electrode configuration designs for impedance-based MFCM, including coplanar electrodes,[114,115] parallel electrodes,[116] and constriction channels.[117] Regardless of the design, the detection principle is similar, where excitations are generated by an electrode and signals are collected by multiple sensing electrodes.

4 Sorting systems for microfluidic flow cytometry

In contemporary flow cytometry, sample sorting is a critical step. The sample sorting in a traditional flow cytometer is accomplished by diverting the charged sample-contained droplets within an electric field. Various on-chip sample sorting methods have been employed in MFCM and they can be generally split into active and passive approaches.[118–120] Active sorting relies on external forces (enabled by electric, magnetic, optical, acoustic, or piezoelectric actuation), while passive separation utilises the internal dynamics (such as specifically designed geometric microstructures in microchannels).[121,122] In this section, we summarise the main sorting approaches and their characteristics in MFCM. Detailed reviews of the sorting methods in MFCM can be found elsewhere.[68,123,124]

4.1 Mechanical sorting systems

Mechanical sorting systems usually rely on external actuators connected to the microfluidic chip. Utilising the piezoelectric effect finds a balance between cost and performance when compared to other actuation approaches. In applications, it offers the benefits of flexibility, disposability, and competitive prices. The piezoelectric lead-zirconate-titanate (PZT) actuator has a very short reaction time and may bend according to the polarity of the electric potential. When a PZT actuator is placed onto a microchip and connected to on-chip dual membrane pumps, it can sort cells using a pull-push relay method to generate lateral flows, as shown in Fig. 4a. The volume and response speed of the local flow is controlled by varying the input signal applied to the PZT actuators.[125,128] The mechanical sorting system can separate both large and small samples, and the viability of cells can be maintained at a high level. However, the throughput and sorting efficiency are influenced by the upstream focusing and detecting systems.

4.2 DEP based sorting systems

As introduced in the focusing section, DEP can also be utilised to separate particles by generating polarisation forces in a non-uniform electric field.[129] A bifurcation configuration is commonly used for sorting targeted samples, such as cell-laden droplets.[69,130–132] In this method, in the absence of the electric field, samples flow into the branch with lower hydrodynamic resistance; during the sorting process, the electrode near the bifurcation is energised to steer the required samples into the collecting channel. Recently, this method was further improved with sequentially addressable dielectrophoretic array (SADA).[126] As shown in Fig. 4b, the SADA sorter delivers an accumulated DEP force to the target droplet using an array of electrodes that can be sequentially activated and deactivated to synchronise to the droplet's speed and position. The droplet can then be gently pulled in the direction of sorting in a high-speed flow. The SADA sorter can sort microdroplets with a large size, which is challenging to achieve using only a single pair of electrodes as the intensive nonuniform electric field required for sorting can fracture the droplet. The DEP based sorting method is more flexible and programmable. However precise fabrication and control requirements limit its application and integration to MFCM.

4.3 Acoustic sorting systems

The acoustophoretic technique for sample sorting is an appealing and biocompatible option. The viability of cells can be maintained for minutes to hours under a low-intensity acoustic field. Furthermore, it's simple to be incorporated into a microchip-based platform. Acoustic waves are generated mainly by piezoelectric actuators,[133] and TSAWs and SSAWs are two main forms of SAWs to achieve the sorting. TSAWs are formed utilising a single pair of interdigital transducers, whereas SSAWs are generated by the interference of two TSAWs.[134] As shown in Fig. 4c,[127] individual particle displacement were achieved by focused SAW enabled acoustic fields. With the microseconds level pulses, 2 μm and larger samples are able to be moved as required and sorting speed can vary from 1 to 10 kHz. The acoustic system is able to increase the sorting throughput because of its short response time and the large driving force makes it capable of sorting samples with various sizes. However, the complex control instruments may lead to bulky systems.

In summary, we briefly introduced various commonly used techniques adopted by MFCM. Based on the physical and biochemical properties exhibited on different blood-based biomarkers, the choice of specific focusing, detecting, and sorting techniques is summarised in Table 2.

5 Microfluidic flow cytometry for blood-based biomarker analysis

Based on the abovementioned key techniques for focusing, detecting, and sorting biological particles, significant developments of MFCMs for analysing biomarkers in blood, including cells, viruses, circulating nucleic acids, and metabolites have been made in recent years, as summarised in Table 3.

5.1 MFCM for detecting cell-based biomarkers

The introduction of circulating tumour cells (CTC) as a minimally invasive multifunctional biomarker has become one of the most exciting discoveries in modern cancer treatment.

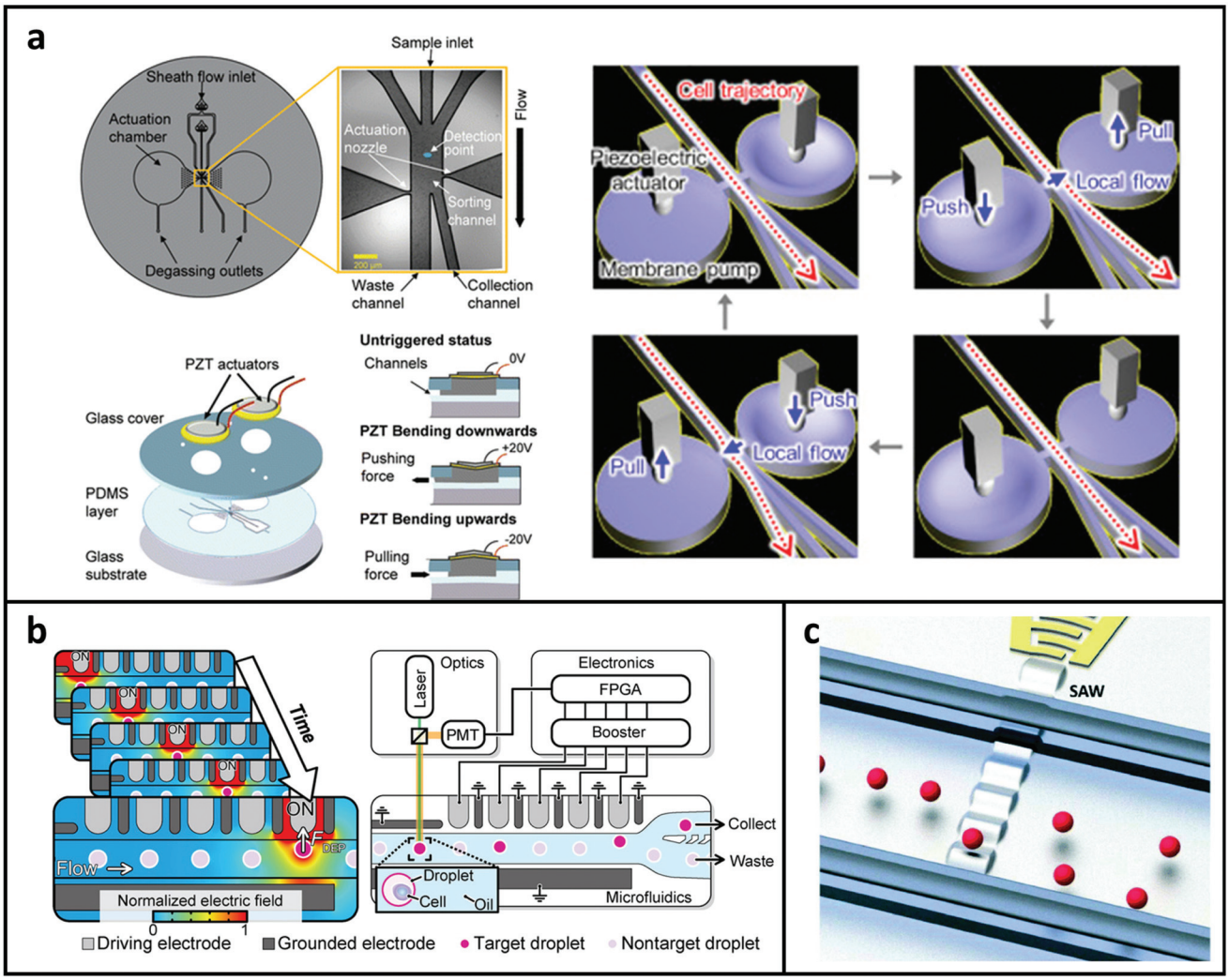

Fig. 4 (a) Illustration of the FACS microchannel based on the mechanical actuation mechanism for sample sorting. (Left) Reproduced from ref. 125 with permission from Springer Nature, copyright 2017. (Right) Reproduced from ref. 86 with permission from Elsevier, copyright 2018. (b) Illustration of the microchannel based on a DEP array for sample sorting. Reproduced from ref. 126 with permission from American Association for the Advancement of Science, copyright 2020. (c) Illustration of the microchannel based on the high-frequency TSAW for sample sorting. Reproduced from ref. 127 with permission from Royal Society of Chemistry, copyright 2016.

Table 2 Guidance of focusing, detecting, and sorting techniques for blood-based biomarkers

Biomarkers	Properties	Focusing	Detecting	Sorting
Circulating nucleic acids	Small size; amplification is required in most applications	Droplets	Optical	Mechanical DEP
Metabolites	Various formats; complex sample preparation process	Droplets	Optical	Mechanical DEP
Cells	Relatively large size; various labelling methods	Hydrodynamic Acoustic DEP Inertial	Optical Image Impedance	Mechanical Acoustic
Viruses	Small size; antibody conjugation is required in most applications	Hydrodynamic (on beads) Droplets	Optical	Mechanical Acoustic

CTCs in the peripheral blood come from solid tumours and are implicated in hematogenous metastatic dissemination to distant areas, allowing secondary foci of illness to form. In one millilitre of blood containing ~1×10^9 blood cells, most individuals with metastatic cancer have less than 10 CTCs. The purpose of CTC technology is to separate and recover individ-

Table 3 Summary of MFCMs applied for blood-based biomarker detection and screening

Biomarker category	Sub-categories	Disease	Separation	Detection method	Throughput	Limit of detection	Remarks	Ref.
Cells	Tumour cells	Cancer	Deterministic lateral displacement (DLD)	Optical based (fluorescent microscope)	5 cells per min	10^4 cells per mL	Enzyme assay	135 and 136
	Circular tumour cells (CTC)	Cancer	N/A	Optical and photoacoustic based (PMT and ultrasound transducer)	15 cells per h	1 cell per 40 mL	Mouse *in vivo* analysis	137 and 138
		Cancer	Mechanical actuation	Optical based (PMT)	3×10^5 cells per min	10 CTC per mL	Labelled mouse tumour cells	139 and 140
		Breast cancer and Nonsmile cell lung cancer	Inertial	Optical based (PMT)	1.2×10^3 particles per h	1×10^3 particles per mL	Human tumour samples	141
		Pancreatic ductal adenocarcinoma	N/A	Impedance based (impedance spectroscope)	~350 cells per s	$\sim 2 \times 10^5$ cells per mL	Human tumour samples	142
		Breast cancer and melanoma	N/A	Impedance based (impedance analyser)	N/A	N/A	Human tissue samples	143–145
	Bacteria	Bacterial infection	N/A	Optical based (fluorescent microscope)	N/A	100 CFU per mL	*E. coli, E. aerogenes, S. aureus*	23 and 146–148
	Fungi	Nosocomial infection	N/A	Optical based (digital PCR)	N/A	10^5 CFU per mL	*Candida albicans*	149
Viruses	Virus particle	Viral infection	N/A	Optical based (PMT)	1.5×10^9 virus per h	3×10^7 virus per ml	Baculovirus	150
		Viral infection	N/A	Impedance based (impedance spectroscope)	10 mL per min	Down to 3 ng mL^{-1} (antigen concentration)		151
		Dengue	N/A	Optical based (PMT)	N/A	10^3 PFU per mL	Dengue virus serotype 2	17
Circulating nucleic acids	Cell-free DNA (cfDNA)	Cancer	N/A	Optical based (digital PCR)	N/A	20 ng per μL	PCR	152–161
		Breast cancer	N/A	Optical based (digital PCR)	N/A	N/A	PCR	162–165
		Colorectal cancer, lung cancer	N/A	Optical based (digital PCR)	N/A	25 ng per μL	PCR	166–169
		Viral infection	N/A	Optical based (digital PCR)	N/A	10 ng per μL	PCR	170–172
		Hepatitis B	N/A	Optical based (digital PCR)	N/A	N/A	PCR	173
		AIDS	N/A	Optical based (digital PCR)	N/A	20 ng per μL	PCR	161 and 174
		Bacterial infection	N/A	Optical based (digital PCR)	N/A	100 CFU per swab	PCR	175 and 176
	RNA	Viral infection	N/A	Optical based (fluorescent microscope)	N/A	N/A	PCR	177
		Hepatitis C	N/A	Optical based (digital PCR)	N/A	0.005% of mutant in the presence of a 20 000-fold excess of the wild-type DNA.	PCR	178
		AIDS	N/A	Optical based (digital PCR)	N/A	N/A	RT-PCR	179
		Bacterial infection	N/A	Optical based (avalanche photodiode)	N/A	10 aM	Enzyme assay	180
		Influenza	N/A	Optical based (fluorescent microscope)	N/A	10 copies per μL	Loop-mediated isothermal amplification (LAMP)	181
Metabolites	Prostate-specific antigen	Prostate cancer	N/A	Optical based (fluorescent microscope)	2×10^5 droplets per chip	~100 pg per mL	Bead-based ELISA	182
	Surface protein	HIV	N/A	Optical based (fluorescent microscope)	200 cell-containing droplets per s	110 fM	Enzyme assay	183
	Matrix metalloproteinase	Endometriosis, breast cancer	N/A	Optical based (fluorescent detection setup)	N/A	5 ng per μL	Enzyme assay	184–188
	β-Galactosidase	Bacterial infection	N/A	Optical based (fluorescent microscope)	~960 cells per min	6.4×10^5 cell per mL	Enzyme assay	182, 189 and 190
	Cellobiohydrolase	Bacterial infection	N/A	Optical based (PMT)	100 μL per h	N/A	Enzyme assay	191
	Glucose oxidase	Diabetes	N/A	Electrochemical based (electrochemical workstation)	3.6 μL per min	0.05 mM	Enzyme assay	192
	β-Glucosidase, catalase, C-reactive protein	Infection, inflammation, cancer	N/A	Optical (PMT)/electrochemical (electrochemical workstation) based	500 droplets per s	0.01 μg per mL	Enzyme assay, antibody conjugation	193–195

ual CTCs or clusters of CTCs in large quantities of whole blood (>5 mL) with excellent purity and low shear stress to avoid cellular damage. Serial evaluations for pharmacodynamic (PD), prognostic, predictive, and intermediate endpoint biomarker research may be performed at numerous life stages during a patient's cancer journey thanks to the development of contemporary CTC technology.[20–22]

CTCs, like blood cells, carry epithelial surface markers, the most common of which are epithelial cell adhesion molecules (EpCAM). Based on this, the 'CTC-chip', the first microfluidic technique to collect CTCs from whole blood, utilised microposts coated with EpCAM antibodies.[140] Although other surface epitopes can be used, such as human epidermal grown factor receptor 2 (HER2) or epidermal growth factor receptor (EGFR), the production of cancer surface markers is very variable, even from the same patient.[196] Because CTCs have such a wide range of expression, microfluidic methods based on an immunoaffinity technique may overlook a significant percentage of CTC cells. Rather than antibodies, aptamer panels can be employed, although these might lack selectivity in detecting CTCs because they were derived from cancer cell lines.[197,198]

CTCs sorting can be achieved according to various differences like volume, density, compressibility, deformability, or electrical impedance to address the limits of positive or affinity-based selection.[199,200] Volume variances have been used to separate individual samples from blood by applying acoustic radiation forces,[199] a mixture of inertial flow and Dean vortex flow,[201] or micro vortices.[202] Recently, with lateral deterministic displacement technology, clusters containing from 2 to 100 cells can be isolated from whole blood.[203,204] While some tumour cells have a larger size compared to leukocytes, a large percentage of CTCs are comparable in size to leukocytes. These approaches, like positive selection, can overlook a significant percentage of CTCs that are roughly comparable to leukocytes.

Hamza *et al.*[139] created an optofluidic real-time cell sorting system that can harvest fluorescently labelled CTCs from a genetically manipulated mouse in a continuous fashion (Fig. 5a). On the back of a mouse, an arteriovenous shunt was inserted, permitting continuous blood extraction from the left carotid artery and return *via* the right jugular vein. A microchip with one input and two outputs was used to link the circulation. The stream channel was lit by two closely separated laser beamlines for recognising fluorescently expressed CTC and determining cell velocity. The circulation was controlled by two valves downstream of the microchannel, which sent it either back to the mouse body or the CTC collecting tube. This approach allows CTCs sorting with small amounts of blood. Fig. 5b illustrates the tumour cells detecting method enabled by the two excitation laser beams. More recently, as shown in Fig. 5c and d, McGrath *et al.*[142] published a thorough research aimed at phenotyping pancreatic tumour xenografts based on tumorigenicity. Individual cells from primary pancreatic tumours and those from liver metastasis were compared utilising a high-throughput system (>300 cells per sec) and an impedance-based phase-contrast criteria, which relies on impedance phase variations in the low and high frequency ranges. Differences in this measure were discovered to be linked to cell interior electrophysiology and to change consistently as a function of tumorigenicity. Furthermore, DEP was conducted simultaneously, confirming that cancer cells with greater tumorigenicity had lower internal conductivity and higher permittivity. The phenotypic characterisation was further validated by genetic investigation, which revealed that dysregulation of Na^+ transportation and Ca^{2+} removal existed in more tumorigenic cell types.

The electrical properties of CTCs were tested with impedance spectroscopy and electrorotation.[143–145] As an example, the impedance of four breast cancer cell lines, MCF-7, MCF-10A, MDA-MB-231, and MDA-MB-435S, was examined by Qiao *et al.*[145] These cell lines range from healthy cells to cancer cells in late stages. They used a microfluidic chip with electrodes attached to an impedance analyser to analyse the cell suspensions. The impedance of cell suspensions was used to obtain the electrical characteristics of single cells, including whole cell conductivity, membrane capacitance, cytoplasm conductivity, and relaxation frequency. Researchers discovered that each cell type has unique electrical characteristics that gives it a feature that may be utilised to differentiate cells and determine the stage of cancerous cells.

In addition to the breast cancer cells, the construction of an interdigitated microelectrode array (IDMEA) biosensor using electrochemical impedance spectroscopy and cyclic voltammetry to examine the B16 melanoma cell line was reported by Avram A. *et al.*[144] They measured the adherence and spread of B16 melanoma cells on IDMEA and developed an impedance spectrum for them. Likewise, Avram M. *et al.*[205] proposed a label-free melanoma cell detection approach depending on the melanoma cells' dielectric characteristics and the gold nanoparticles (AuNPs) within. C57BL/6 mice were injected with 1×10^6 murine melanoma B16 cells dispersed in 0.1 mL PBS. The mice received 200 μL of 200 nM AuNPs suspended in PBS intravenously. The investigators discovered a significant difference in the scattering spectra of AuNPs in melanoma cells and AuNPs in normal tissue during histopathological investigation of the tumour tissue. The B16 melanoma cells containing AuNPs in cytoplasm showed a distinct blue colour under ultraviolet fluorescence, which was associated with the localised surface plasmon resonance (LSPR) principle. This technology might be used to diagnose patients without the usage of labels.

Most MFCMs for single cell-derived biomarker detection rely on immortalised cell lines in controlled buffers or reference bacterial strains in controlled buffers/broth. For a few platforms that process clinical biofluids, each requires varying degrees of off-chip or on-chip sample preparation. Therefore, integrating sample process modules into the platform might be a feasible way to minimise and automate MFCM systems. However, the downsides of such an approach are added assay complexity and difficulty in platform design, fabrication, and control. As such, both the advantages and the disadvantages

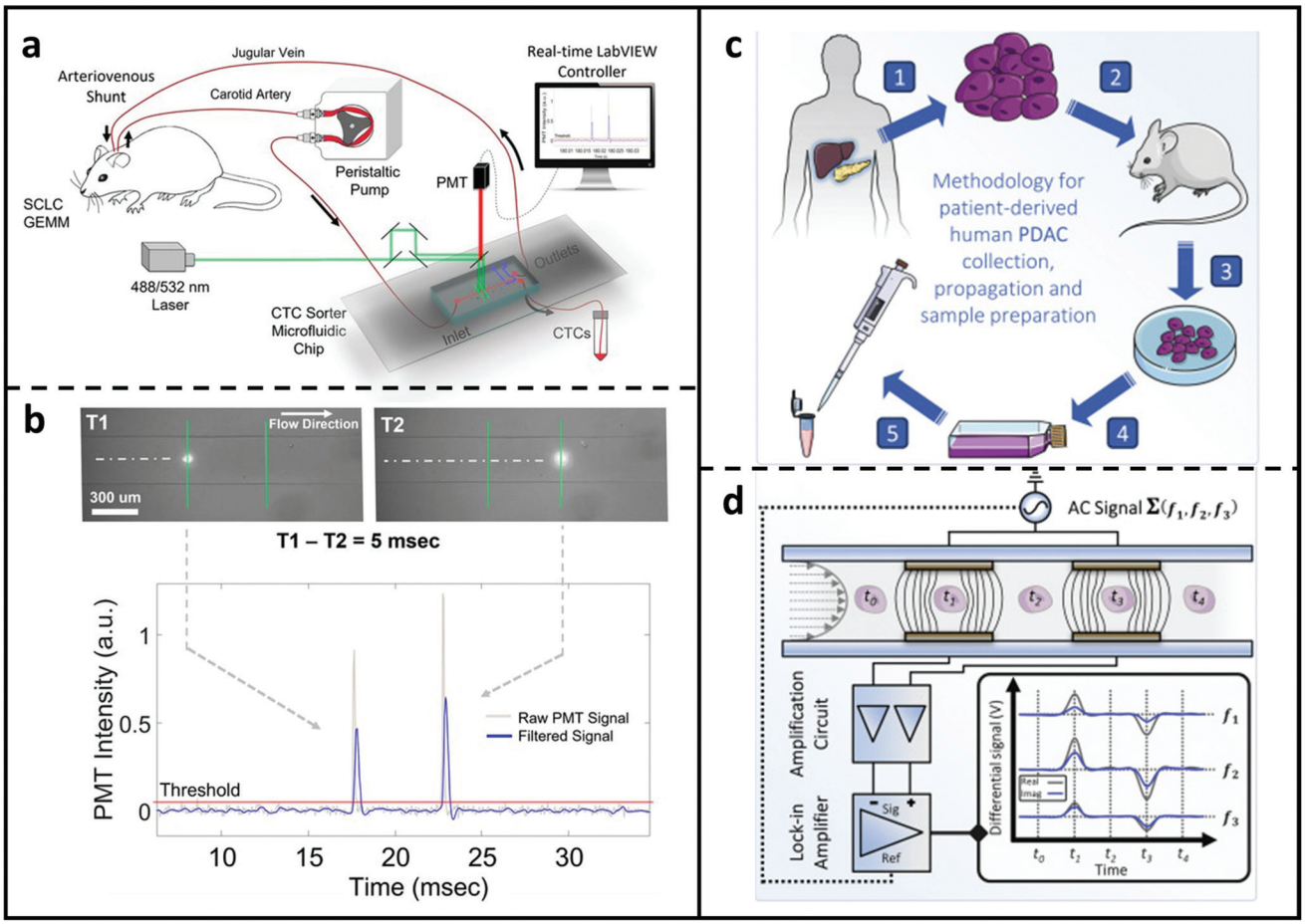

Fig. 5 MFCMs for detecting cancer cells. (a) Microfluidic sorter for CTC studies in genetically engineered mouse models. Peristaltic pump extracts body fluids from a mouse and the blood were pumped into the sorter microchip. A fluorescence-based sorting system was used to collect rare CTC cells, and the processed blood redirected to the vein. (b) Schematic of the CTC detecting module containing two excitation laser beams. Reproduced from ref. 139 with permission from National Academy of Science, copyright 2019. (c) Workflow from Pancreatic ductal adenocarcinoma (PDAC) patient to microchip *via* the xenograft (PDX) model. (1) Tumour cells collected from patients with PDAC and (2) implanted and propagated in immunocompromised mice as a PDX. (3) After that, PDAC samples were created from surgically removed PDX and (4) cultured in medium at 37 °C. (5) Aspirated PDAC cells were then cleaned and restored in solution used for impedance cytometry. (d) Illustration of the impedance-based detecting process. PDAC tumour cells suspension was driven through the detection channel which includes two pairs of facing microelectrodes. Voltages at three discrete frequencies were applied to the top electrodes and the differential current were amplified and acquired at the bottom electrodes. Reproduced from ref. 142 with permission from Elsevier, copyright 2020.

will have to be carefully evaluated for obtaining optimal platform performance.

5.2 MFCM for detecting bacteria, fungi, and microorganisms

Rapid and reliable identification of low abundance pathogens in biological samples is critical for disease diagnosis and subsequent therapeutic arrangements in infectious diseases. As shown in Fig. 6a, Kaushik *et al.*[23] introduced a fast and integrated method. The researchers used 20 pL microdroplets to encapsulate a single bacterium. Because of the lower background in the smaller droplets, the fluorescence signal formed by bacterial growth could be determined more rapidly. The effect of gentamicin on the development of a susceptible and multidrug resistant strain of *E. coli* was found after just ~1 hour, which is comparable to two to three bacterial doubling occurrences. Instead of using droplets, Rho *et al.*[151] demonstrated the utilisation of microbeads, as shown in Fig. 6b, in which an MFCM was used for complex immunoassay using gold microspheres tethered to a filamentous virus. This technique enabled a high number of antibodies to be attached to the microspheres while also reducing non-specific adsorption. The researchers used MFCM with fluorescence and DC-impedance to detect four distinct biomarkers at the same time: cardiac troponin I (cTnI), prostate specific antigen (PSA), creatine kinase MB (CK-MB), and myoglobin. The detection limit of virus-tethered beads was higher than that of virus-free beads.

Faez *et al.*[206] presented a technique that can trace unlabelled dielectric nanoparticles as tiny as 20 nm, at speeds of over 3 kHz for tens of seconds (Fig. 6c). A single-mode, step-

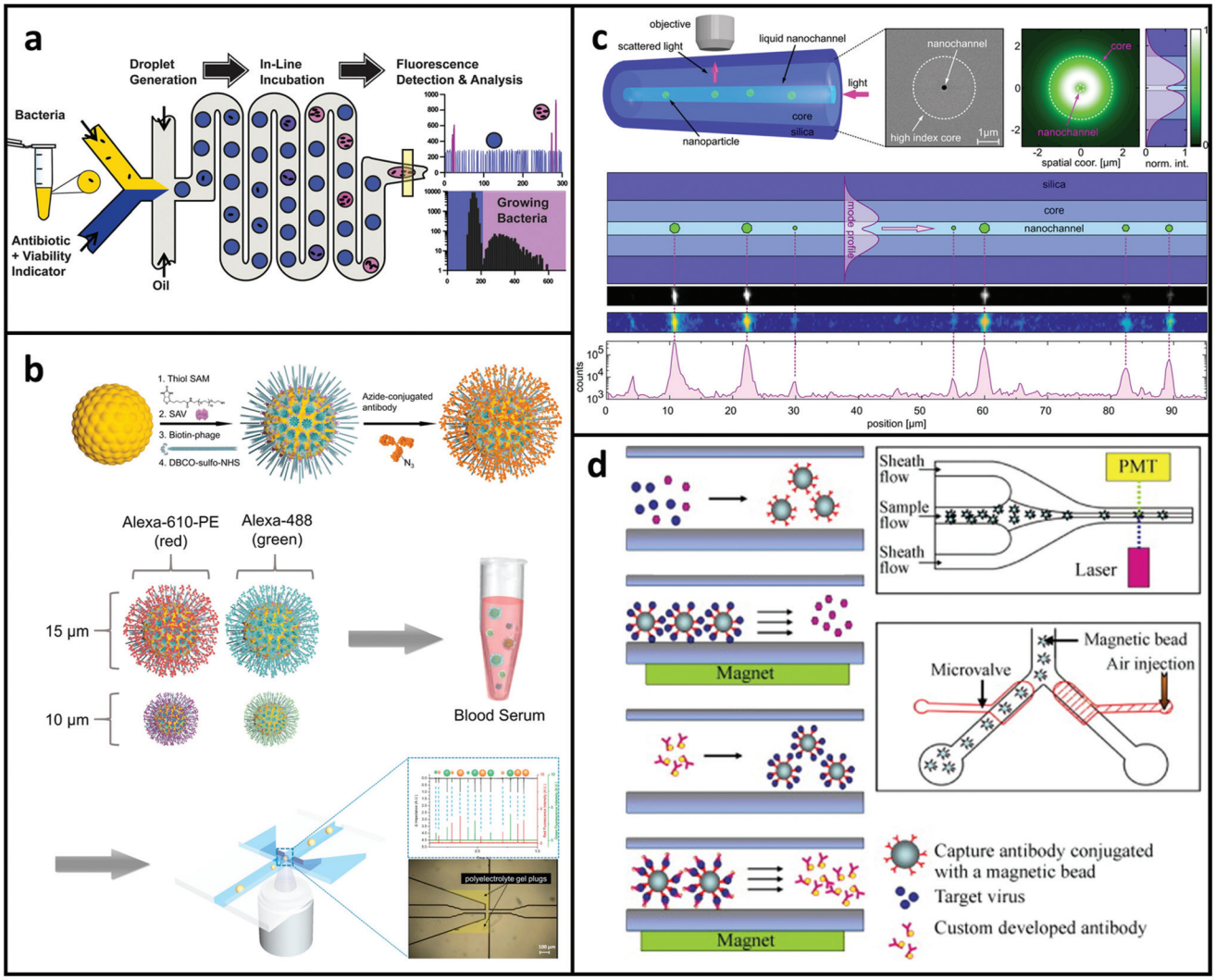

Fig. 6 MFCM analysis for detecting pathogen biomarkers. (a) Illustration of one-step platform for bacterial growth testing and antibiotic susceptibility examination. Reproduced from ref. 23 with permission from Elsevier, copyright 2017. (b) Illustration of the surface modification workflow for bio-inspired filamentous virus tethered on gold-layered beads. Reproduced from ref. 151 with permission from Elsevier, copyright 2018. (c) Detection of dielectric nanoparticles in a nanofluidic fibre. Reproduced from ref. 206 with permission from American Chemical Society, copyright 2015. (d) MFCM for rapid virus detection. Reproduced from ref. 17 with permission from Elsevier, copyright 2008.

index optical fibre with an open nanosised path inside the high-index core is the fundamental component of the technology. The particles were suspended in a solution that fills this channel. The laser was then directed through the centre of the fibre. A part of the optical mode in the fibre overlaps with the nanochannel cross-sectional area since the tube size is smaller than the light wavelength. The directed light scattered off the particles, passed through the transparent fibre cladding, and was captured by a microscope objective positioned vertical to the fibre axis. Although using optical fibres allows detecting nanoparticles without labelling, the rather sophisticated setup makes it difficult to be adapted for other applications. In another example, a MFCM has been developed with functional micro-devices capable of detecting and collecting viral particles.[17] The proposed method effectively recognised a dengue virus sample with a concentration of 1000 PFU ml^{-1} in experimental findings. Fig. 6d illustrates the experimental processes using the MFCM. Surface-coated with streptavidin and conjugated with biotinylated capture antibodies, superparamagnetic beads with a diameter of 6 μm were combined with biosamples in the incubation system. The targeted viruses can be collected and attached to the antibody-conjugated magnetic microspheres in a specified manner. After an on-chip washing process, the second set of prepared antibodies was mixed with the purified samples and cultivated with fluorescent dye to determine the target viruses. A microfluidic hydrodynamic focusing subsystem was used to drive the refined virus-magnetic-bead compounds. Following that, an optical detection system consisting of a laser generator as well as a photo-multiplier tube was used to stimulate and measure the fluorescent signal coupled to the second antibodies on the specific viruses. Finally, utilising the feedback signals from the optical

detector, a sorting module (active microvalves) positioned downstream would sort and harvest virus-bound magnetic beads into the collecting chambers.

Rane *et al.*[207] proposed a method without amplification for detecting pathogen-specific rRNA in individual bacterial samples. For counting *E. coli* spiked into suspensions, the investigators encapsulated single *E. coli* cells into 10-pL sized microdroplets and utilised a 16S rRNA-specific peptide nucleic acid (PNA) probe. This method could detect *E. coli* in low concentrations (equivalent to 5×10^6 CFU mL^{-1}) and could perform continuously for higher throughput and dynamic range. Also, Kang *et al.*[208] employed a DNAzyme sensor to detect *E. coli* spiked in 10% blood to prove the possibility of direct clinical sample analysis. Individual bacterial cells were enclosed in droplets with a volume of 14 pL and a diameter of 30 μm. The platform might produce a positive/negative result for the existence of the bacteria being examined after 45 minutes of lysis and DNAzyme response. The system was capable of evaluating dilute of *E. coli* from 1 to 10^4 CFU mL^{-1} after 3.5 hours. While fast bacterial detection for *E. coli* has been achieved using microdroplets with higher sensitivity, additional work is needed to enhance the capabilities of technologies to assess the presence of other pathogenic specimens. Furthermore, whereas the aforementioned systems have already shown pathogen identification with precultured *E. coli*, a droplet-based method that could instantly analyse culture-positive clinical samples has not been proven.

5.3 MFCM for detecting circulating nucleic acids

Dying cells can release cell-free DNA (cfDNA) and other nucleic acid fragments, possibly by active secretion.[210] Tumour cells release mutant cfDNA, also called circulating tumour DNA (ctDNA), which is currently considered a marker and has been utilised as a prognostic diagnostic for several malignancies.[14] The short half-life of cfDNA, ranging from 6 min to 2.5 hours, makes it useful for monitoring pharmacological treatment response. cfDNA levels in blood vary from 1–10 ng mL^{-1} in healthy people, but they can reach 1000 ng mL^{-1} in patients with cancer, equating to 3000–360 000 mark genes per millilitre of plasma.[209,211] High cfDNA levels, on the other hand, can become a sign of inflammation, benign tumours, or tissue damaging.[211] While cfDNA has received the greatest attention due to its reliability, cell-free mRNA, microRNA, nucleosomes, and viral DNA are all being explored.[210]

As shown in Fig. 7a–c, a multiplexed digital PCR platform was introduced by RainDance Technologies for measuring six specific somatic mutations related to colorectal cancer in the Kirsten rat sarcoma virus (KRAS) oncogene at the same time.[209] This approach could screen millions of responses from a single sample while consuming less reagent per sample owing to the use of picolitre droplets. Additionally, the researchers were capable of checking each sample for six mutations at the same time by optically coding individual probe microdroplets with different quantities of fluorescent dye and passively combing the sample and the probe microdroplets. Commercial product, RainDrop, from RainDance Technologies has been employed for tracking mutations in KRAS for colorectal cancer[167] as well as EGFR for lung cancer,[153] B-type Raf kinase (BRAF) for Langerhans cell histiocytosis,[152] and a 5-plex genotyping assay for spinal muscular atrophy.[166] However, practically all clinical droplet digital PCR solutions have depended on an additional benchtop procedure for nucleic acid extraction and purification before droplets production. Several microfluidic technologies have been introduced to better enhance and incorporate DNA extraction into the microfluidic PCR process.[212–214] Despite this, none of these systems has been included in droplet digital PCR procedures. As a result, additional incorporation of sample preparation processes is required to fully realise the sample-in-answer-out potential of microdroplet-enabled systems.

Custom droplet PCR technologies for detecting viral nucleic acids have also been established, with an emphasis on speed, quantification, and integration. Kiss *et al.*[170] established a combined solution to amplify and measure adenoviral DNA in 65-pL microdroplets. The researchers were able to screen millions of interactions in a continuous manner and identify signals from amplification in as short as 35 minutes enabled by the incorporation of the micro-sized droplets and the optimisation of the workflow procedures within a single platform. Furthermore, the platform's parallel sample interrogation regions enabled the production of real-time PCR fluorescence curves. While this study established quantification of the pAdeasy-1 adenoviral vector, a sensitive RNA quantification system is necessary for additional clinically relevant viral load testing, such as HIV-1 and HCV. To this end, Rački *et al.*[215] designed a rotavirus quantification method that achieved viral RNA extraction, reverse transcription, and on-chip droplet digital PCR to measure viral RNA in wastewater. While custom platforms can be designed to be fully integrated and automated, the relatively small device footprint limits the throughput to roughly 100 droplets per experiment. Guan *et al.*[180] established a more comprehensive platform than the earlier study, which used a platform without amplification for absolute bacterial (*N. gonorrhoea*) rRNA quantification. An enzyme-linked oligonucleotide hybridization assay (ELOHA) for quantification of RNA was established in this research, which enabled RNA molecules to hybridise onto DNA catching probes which were coupled to magnetic microspheres. The collected RNA was then hybridised with enzyme-labelled detecting probes. After that, the microspheres were enveloped in microdroplets with a fluorogenic substrate for further identification and evaluation. Quantification of nucleic acid-laden microspheres using ELOHA yielded great accuracy (CV 10%) over a rather large dynamic range spanning three orders of magnitude (Fig. 7d). Compared to traditional amplification techniques for detecting nucleic acids, the work utilising droplets presents a unique opportunity to detect nucleic acids without the need for target or signal amplification, which provides an alternative to overcome limits including low amplification efficiency, susceptibility to contamination, and long thermocycling duration.

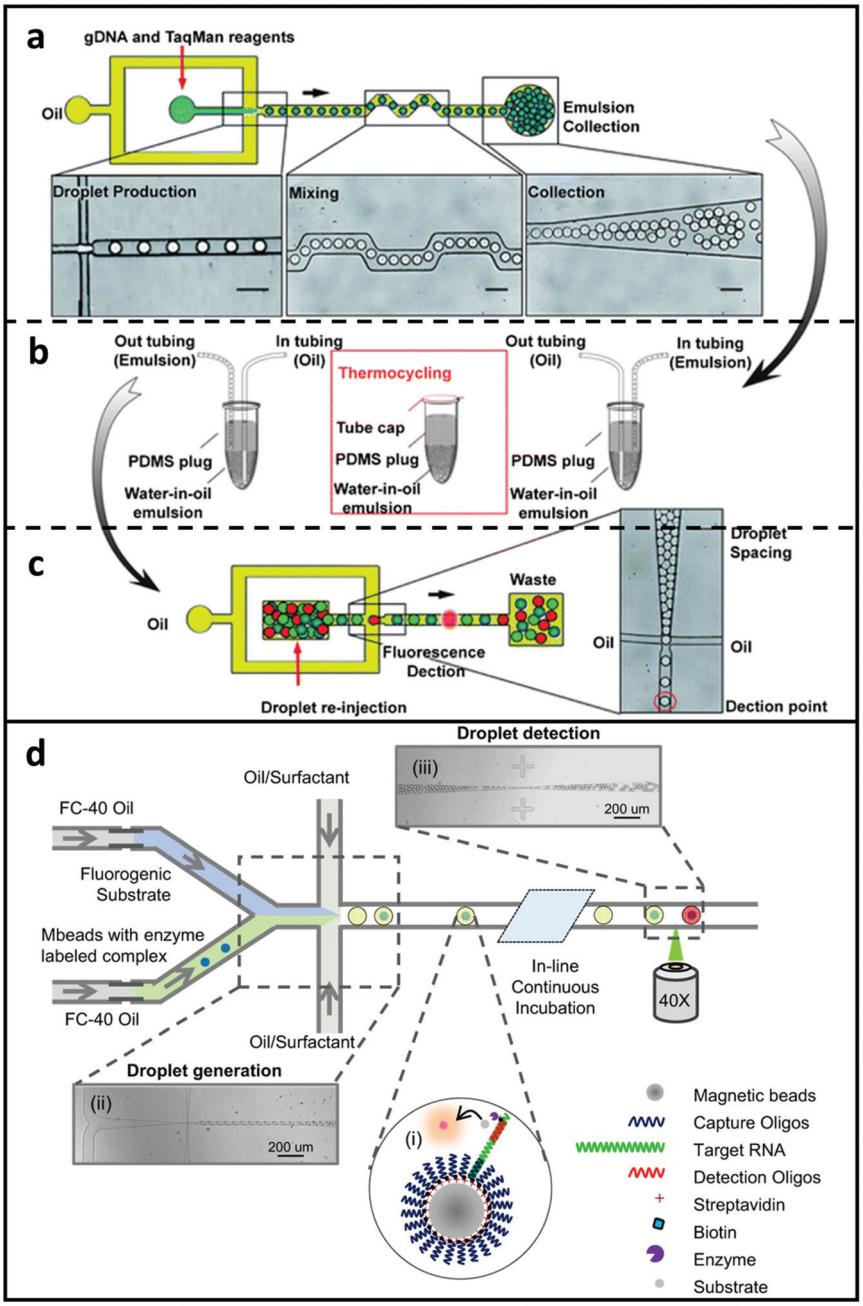

Fig. 7 Droplet-based MFCM for detecting nucleic acid biomarkers. (a–c) Illustrations of a microdroplet digital PCR platform for mutations screening in the KRAS oncogene. TaqMan probes and mutant genes were enclosed in microdroplets with just one haploid genome each. After that, the droplets were thermocycled and re-introduced for fluorescence detecting. This technology was used to identify six different mutations in KRAS at the same time by optically coding droplet groups. Reproduced from ref. 209 with permission from Royal Society of Chemistry, copyright 2011. (d) Co-flowed into droplets with appropriate enzyme substrate forms a sandwiched complex comprising of capture oligo-coated magnetic microspheres hybridised to a single molecule of specific RNA, which is subsequently hybridised to an enzyme-linked detection oligo. Microdroplets containing individual RNA glow brightly after incubation, while microdroplets without the sandwiched complex fluoresce dimly. Reproduced from ref. 180 with permission from Springer Nature, copyright 2015.

5.4 MFCM for detecting metabolites

Microfluidic systems have been introduced for low-abundance protein biomarker detection as well as multiplexed protein biomarker testing and analysis. This is then utilised in disease screenings for bacterial infections, cancer, diabetes, and endometriosis, amongst other things.

Droplet systems provide the ability to improve the LoD of enzyme-linked immunosorbent assays (ELISAs), which have become a gold standard for protein detecting at high sensi-

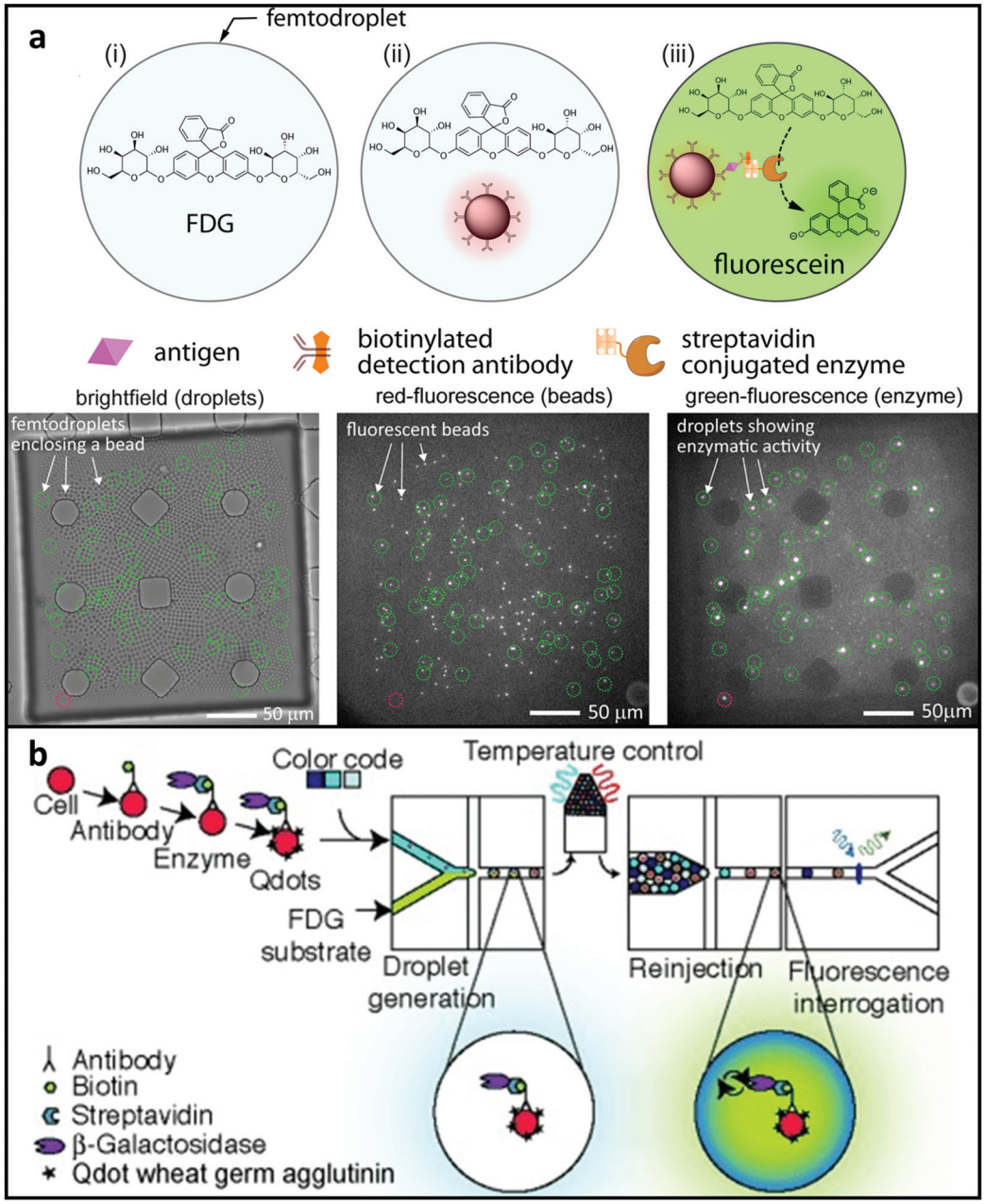

Fig. 8 MFCM for detecting metabolites. (a) Illustration of a platform enabled by microsphere-based sandwich assay for PSA quantifying. The target protein was labelled by a reporter enzyme and hybridised to the microspheres and then modified microspheres and substrate were encapsulated together with microdroplets. Low concentration protein biomarkers can then be detected after incubation. Reproduced from ref. 182 with permission from American Chemical Society, copyright 2015. (b) Illustration of microdroplet MFCM using an enzyme-tagged antibody to screen the low-abundance cell-surface protein biomarker CCR5 in U937 cells. Reproduced from ref. 183 with permission from John Wiley and Sons, copyright 2009.

tivity. In an ELISA test, proteins coupled to enzymes are conjugated to antibodies immobilised on the substrate surface or a dispersed microsphere.[18] After protein conjugating, a fluorogenic substrate is added into the mixture, and proteins may be identified after processing by enzyme–substrate cleavage. A tagged secondary antibody can also be employed for identification. In order to multiplex analyte detecting, commercial immunoassay technologies rely on microbeads with optically coding or customising microarrays.[19] Because of the natural intricacy in the production of microspheres or micro-scale arrays, most of these systems are costly and require a lot of supporting equipment.

The sensitivity of bulk ELISA tests is often restricted to picomolar concentrations or higher. Protein biomarkers might be in significantly lower concentrations for several disorders, such as prostate cancer.[216] To meet this demand, Shim

et al.[182] designed a system using femtoliter droplets for single-molecule counting immunoassays. In this study, antibody-functionalised catch microspheres were combined with the target protein in PBS until each microsphere contained 0 or 1 copy of the target molecule. Next, the trapped proteins were then coupled with a detection antibody, followed by the streptavidin-conjugated β-galactosidase reporter enzyme. 2×10^4 microdroplets were produced that laden bead-analyte-enzyme complex and a fluorogenic substrate. Microspheres carrying the analyte–enzyme combination combined with the fluorogenic substrate began to glow shortly after microdroplet generation. Signals from microdroplets carrying single-molecule can be recognised by imaging utilising a CCD sensor after a quick 10-minute on-chip incubation process (shown in Fig. 8a). The scientists utilised their technology to identify PSA at 46 fM concentrations, which is much lower than bulk ELISA. The scientists also suggest that it is possible to easily scale up the incubating zone and detecting method to enhance dynamic range and perhaps minimise LoD. Droplets can also recognise low-abundance surface proteins. Joensson *et al.*[183] described a technique for screening mammalian cells for the low-abundance surface protein CCR5, which is a biomarker for HIV-1 infection (Fig. 8b). Enzyme-tagged antibodies were combined with fluorogenic substrates inside microdroplets with diameters of 40 μm to mark the cells. The droplets were re-injected and identified after being incubated off-chip, and they demonstrated higher resolution for distinguishing cells expressing CCR5 than typical FACS-based approaches. In the above-mentioned molecular biomarker detecting platforms, the enhanced sensitivity requires mechanisms for rejecting assay inhibitors and sources of false-positive signals. To this end, samples may be prepared prior to encapsulation in droplets, such that the background molecules responsible for assay inhibition or false-positive signals are minimised or even completely removed. Most current droplet-based platforms have achieved high sensitivity by relying on some degree of off-chip sample preparation and/or biomarker purification. Therefore, one important future investigation should be the integration of on-chip sample preparation process to purify the sample or concentrate the target biomarkers prior to droplet generation.

6 Conclusion and perspective

Over the past decade, benefitting from achievements in various technologies such as microfabrication and artificial intelligence, great efforts have been made in the development of MFCM including each subsystem, offering a promising future to make the MFCM achieve better performance in accuracy, cost, and throughput. This review has described the key submodules in a typical MFCM including focusing, detecting, and sorting systems. For each method presented, the characteristics and principles have been described and explained. In addition, the application of MFCM in blood-based biomarkers, such as cell-based and circulating nucleic acids-based has also been reviewed. Overall, this review offers a meaningful summary of the recent advances in microfluidic flow cytometers and their demonstration in blood-based biomarker analysis.

Despite a wide range of promising applications of MFCM, several under-developed and unsolved issues hinder fully unleashing its capabilities. Numerous on-chip platforms rely on bulky, expensive external supporting instruments. For example, the use of sheath flow for hydrodynamic focusing is unable to be achieved without several high-precision syringe pumps; fluorescence-based detecting systems require powerful laser modules and photodetectors. Integrated systems with novel microfluidic techniques such as SAWs or DEP have great potential in focusing and sorting systems without the need for bulky external equipment; however, the performance (*e.g.*, throughput, reliability, repeatability) of such systems needs to be further characterised and improved. Image-based detection systems in MFCM attracts researchers' attention due to the recent advances in artificial intelligence technology and because they contain high dimensional information, which may be a superior way forward for MFCM; however, powerful computers or field-programmable gate array (FPGA) modules with advanced processing capability and fast memories are needed to handle a significant amount of image data. In addition, existing commercial MFCM has not yet proven significant advantages over existing cytometry systems in terms of size and cost. Hence, more efforts and breakthroughs based on existing technologies are required to reduce the size, cost, and complexity of systems to realise low-cost POCT applications.

Author contributions

S.-Y.T. and J.G. proposed the review idea. Y.Z. and S.-Y.T. structured the review. S.-Y.T. and J.G. supervised the student. Y.Z. and Y. Zhao completed and edited the first draft and revised manuscript. All authors participated in writing the manuscript. All authors have read and agreed to the published version of the manuscript.

Conflicts of interest

The authors declare no conflict of interest.

Acknowledgements

This research received no external funding.

References

1 Y. Gong, N. Fan, X. Yang, B. Peng and H. Jiang, *Electrophoresis*, 2019, **40**, 1212–1229.

2 T. Haselgrübler, M. Haider, B. Ji, K. Juhasz, A. Sonnleitner, Z. Balogi and J. Hesse, *Anal. Bioanal. Chem.*, 2014, **406**, 3279–3296.
3 G. M. Whitesides, *Nature*, 2006, **442**, 368.
4 M. Li, H. Liu, S. Zhuang and K. Goda, *RSC Adv.*, 2021, **11**, 20944–20960.
5 R.-J. Yang, L.-M. Fu and H.-H. Hou, *Sens. Actuators, B*, 2018, **266**, 26–45.
6 A. Rajawat and S. Tripathi, *Biomed. Eng. Lett.*, 2020, **10**, 241–257.
7 S. Nahavandi, S. Baratchi, R. Soffe, S.-Y. Tang, S. Nahavandi, A. Mitchell and K. Khoshmanesh, *Lab Chip*, 2014, **14**, 1496–1514.
8 J. Luo, C. Chen and Q. Li, *Electrophoresis*, 2020, **41**, 1450–1468.
9 J. L. Garcia-Cordero and S. J. Maerkl, *Curr. Opin. Biotechnol.*, 2020, **65**, 37–44.
10 C. D. Chin, T. Laksanasopin, Y. K. Cheung, D. Steinmiller, V. Linder, H. Parsa, J. Wang, H. Moore, R. Rouse, G. Umviligihozo, E. Karita, L. Mwambarangwe, S. L. Braunstein, J. van de Wijgert, R. Sahabo, J. E. Justman, W. El-Sadr and S. K. Sia, *Nat. Med.*, 2011, **17**, 1015–1019.
11 H. Chen, K. Liu, Z. Li and P. Wang, *Clin. Chim. Acta*, 2019, **493**, 138–147.
12 M. Sonker, V. Sahore and A. T. Woolley, *Anal. Chim. Acta*, 2017, **986**, 1–11.
13 A. M. Kaushik, K. Hsieh and T.-H. Wang, *WIREs Nanomed. Nanobiotechnol.*, 2018, **10**, e1522.
14 C. Bettegowda, M. Sausen, R. J. Leary, I. Kinde, Y. Wang, N. Agrawal, B. R. Bartlett, H. Wang, B. Luber, R. M. Alani, E. S. Antonarakis, N. S. Azad, A. Bardelli, H. Brem, J. L. Cameron, C. C. Lee, L. A. Fecher, G. L. Gallia, P. Gibbs, D. Le, R. L. Giuntoli, M. Goggins, M. D. Hogarty, M. Holdhoff, S.-M. Hong, Y. Jiao, H. H. Juhl, J. J. Kim, G. Siravegna, D. A. Laheru, C. Lauricella, M. Lim, E. J. Lipson, S. K. N. Marie, G. J. Netto, K. S. Oliner, A. Olivi, L. Olsson, G. J. Riggins, A. Sartore-Bianchi, K. Schmidt, L.-M. Shih, S. M. Oba-Shinjo, S. Siena, D. Theodorescu, J. Tie, T. T. Harkins, S. Veronese, T.-L. Wang, J. D. Weingart, C. L. Wolfgang, L. D. Wood, D. Xing, R. H. Hruban, J. Wu, P. J. Allen, C. M. Schmidt, M. A. Choti, V. E. Velculescu, K. W. Kinzler, B. Vogelstein, N. Papadopoulos and L. A. Diaz, *Sci. Transl. Med.*, 2014, **6**, 224ra224.
15 G. Wen, T. Zhou and W. Gu, *Protein Cell*, 2021, **12**(12), 911–946.
16 P. S. Mitchell, R. K. Parkin, E. M. Kroh, B. R. Fritz, S. K. Wyman, E. L. Pogosova-Agadjanyan, A. Peterson, J. Noteboom, K. C. O'Briant, A. Allen, D. W. Lin, N. Urban, C. W. Drescher, B. S. Knudsen, D. L. Stirewalt, R. Gentleman, R. L. Vessella, P. S. Nelson, D. B. Martin and M. Tewari, *Proc. Natl. Acad. Sci. U. S. A.*, 2008, **105**, 10513–10518.
17 S.-Y. Yang, K.-Y. Lien, K.-J. Huang, H.-Y. Lei and G.-B. Lee, *Biosens. Bioelectron.*, 2008, **24**, 855–862.
18 P. J. Tighe, R. R. Ryder, I. Todd and L. C. Fairclough, *Proteomics – Clin. Appl.*, 2015, **9**, 406–422.
19 S. X. Leng, J. E. McElhaney, J. D. Walston, D. Xie, N. S. Fedarko and G. A. Kuchel, *J. Gerontol., Ser. A*, 2008, **63**, 879–884.
20 T. A. Yap, D. Lorente, A. Omlin, D. Olmos and J. S. de Bono, *Clin. Cancer Res.*, 2014, **20**, 2553–2568.
21 J. S. Ankeny, C. M. Court, S. Hou, Q. Li, M. Song, D. Wu, J. F. Chen, T. Lee, M. Lin, S. Sho, M. M. Rochefort, M. D. Girgis, J. Yao, Z. A. Wainberg, V. R. Muthusamy, R. R. Watson, T. R. Donahue, O. J. Hines, H. A. Reber, T. G. Graeber, H. R. Tseng and J. S. Tomlinson, *Br. J. Cancer*, 2016, **114**, 1367–1375.
22 D. C. Danila, K. Pantel, M. Fleisher and H. I. Scher, *Cancer J.*, 2011, **17**, 438–450.
23 A. M. Kaushik, K. Hsieh, L. Chen, D. J. Shin, J. C. Liao and T.-H. Wang, *Biosens. Bioelectron.*, 2017, **97**, 260–266.
24 Y.-F. Lee, K.-Y. Lien, H.-Y. Lei and G.-B. Lee, *Biosens. Bioelectron.*, 2009, **25**, 745–752.
25 H. Inan, S. Wang, F. Inci, M. Baday, R. Zangar, S. Kesiraju, K. S. Anderson, B. T. Cunningham and U. Demirci, *Sci. Rep.*, 2017, **7**, 3322.
26 S. Yan and D. Yuan, *Talanta*, 2021, **221**, 121401.
27 X. Xuan, J. Zhu and C. Church, *Microfluid. Nanofluid.*, 2010, **9**, 1–16.
28 T. Zhang, Z.-Y. Hong, S.-Y. Tang, W. Li, D. W. Inglis, Y. Hosokawa, Y. Yalikun and M. Li, *Lab Chip*, 2020, **20**, 35–53.
29 L.-M. Fu, C.-H. Tsai and C.-H. Lin, *Electrophoresis*, 2008, **29**, 1874–1880.
30 R.-J. Yang, H.-H. Hou, Y.-N. Wang, C.-H. Lin and L.-M. Fu, *Biomicrofluidics*, 2012, **6**, 034110.
31 J. Kim, J. Lee, C. Wu, S. Nam, D. Di Carlo and W. Lee, *Lab Chip*, 2016, **16**, 992–1001.
32 X. Wang, M. Zandi, C.-C. Ho, N. Kaval and I. Papautsky, *Lab Chip*, 2015, **15**, 1812–1821.
33 J. Zhou, P. V. Giridhar, S. Kasper and I. Papautsky, *Lab Chip*, 2013, **13**, 1919–1929.
34 N. Xiang, X. Zhang, Q. Dai, J. Cheng, K. Chen and Z. Ni, *Lab Chip*, 2016, **16**, 2626–2635.
35 L.-L. Fan, X.-K. He, Y. Han, J. Zhe and L. Zhao, *J. Micromech. Microeng.*, 2015, **25**, 035020.
36 I. D. Johnston, M. B. McDonnell, C. K. L. Tan, D. K. McCluskey, M. J. Davies and M. C. Tracey, *Microfluid. Nanofluid.*, 2014, **17**, 509–518.
37 D. Yang, H. Zou, W. Zhong and T. Xu, *Microelectron. Eng.*, 2015, **139**, 48–52.
38 A. J. Chung, D. R. Gossett and D. Di Carlo, *Small*, 2013, **9**, 685–690.
39 A. J. Chung, D. Pulido, J. C. Oka, H. Amini, M. Masaeli and D. Di Carlo, *Lab Chip*, 2013, **13**, 2942–2949.
40 J.-S. Park, S.-H. Song and H.-I. Jung, *Lab Chip*, 2009, **9**, 939–948.
41 N. Hashemi, J. P. B. Howell, J. S. Erickson, J. P. Golden and F. S. Ligler, *Lab Chip*, 2010, **10**, 1952–1959.

42 J. Zhang, S. Yan, D. Yuan, G. Alici, N.-T. Nguyen, M. E. Warkiani and W. Li, *Lab Chip*, 2016, **16**, 10–34.
43 J. Oakey, R. W. Applegate, E. Arellano, D. D. Carlo, S. W. Graves and M. Toner, *Anal. Chem.*, 2010, **82**, 3862–3867.
44 W. Tang, D. Tang, Z. Ni, N. Xiang and H. Yi, *Anal. Chem.*, 2017, **89**, 3154–3161.
45 W.-P. Chou, H.-M. Wang, J.-H. Chang, T.-K. Chiu, C.-H. Hsieh, C.-J. Liao and M.-H. Wu, *Sens. Actuators, B*, 2017, **241**, 245–254.
46 H. Sadeghian, Y. Hojjat and M. Soleimani, *J. Electrost.*, 2017, **86**, 41–49.
47 Z. Zhu, X. Xu, L. Fang, D. Pan and Q.-a. Huang, *Sens. Actuators, B*, 2016, **235**, 515–524.
48 A. Salari and M. Thompson, *Sens. Actuators, B*, 2018, **255**, 3601–3615.
49 C.-H. Lin, G.-B. Lee, L.-M. Fu and B.-H. Hwey, *J. Microelectromech. Syst.*, 2004, **13**, 923–932.
50 A. Fakhfouri, C. Devendran, T. Albrecht, D. J. Collins, A. Winkler, H. Schmidt and A. Neild, *Lab Chip*, 2018, **18**, 2214–2224.
51 I. Leibacher, S. Schatzer and J. Dual, *Lab Chip*, 2014, **14**, 463–470.
52 I. Leibacher, P. Reichert and J. Dual, *Lab Chip*, 2015, **15**, 2896–2905.
53 B. Ayan, A. Ozcelik, H. Bachman, S.-Y. Tang, Y. Xie, M. Wu, P. Li and T. J. Huang, *Lab Chip*, 2016, **16**, 4366–4372.
54 G. Destgeer, J. H. Jung, J. Park, H. Ahmed, K. Park, R. Ahmad and H. J. Sung, *RSC Adv.*, 2017, **7**, 22524–22530.
55 Z. Ma, Y. Zhou, D. J. Collins and Y. Ai, *Lab Chip*, 2017, **17**, 3176–3185.
56 J. Lee, C. Rhyou, B. Kang and H. Lee, *J. Phys. D: Appl. Phys.*, 2017, **50**, 165401.
57 Z. Mao, Y. Xie, F. Guo, L. Ren, P.-H. Huang, Y. Chen, J. Rufo, F. Costanzo and T. J. Huang, *Lab Chip*, 2016, **16**, 515–524.
58 R. Kishor, Z. Ma, S. Sreejith, Y. P. Seah, H. Wang, Y. Ai, Z. Wang, T.-T. Lim and Y. Zheng, *Sens. Actuators, B*, 2017, **252**, 568–576.
59 D. J. Collins, Z. Ma, J. Han and Y. Ai, *Lab Chip*, 2017, **17**, 91–103.
60 Z. Ma, D. J. Collins and Y. Ai, *Anal. Chem.*, 2016, **88**, 5316–5323.
61 C. Devendran, K. Choi, J. Han, Y. Ai, A. Neild and D. J. Collins, *Lab Chip*, 2020, **20**, 2674–2688.
62 M. Wu, K. Chen, S. Yang, Z. Wang, P.-H. Huang, J. Mai, Z.-Y. Li and T. J. Huang, *Lab Chip*, 2018, **18**, 3003–3010.
63 A. A. Nawaz, X. Zhang, X. Mao, J. Rufo, S.-C. S. Lin, F. Guo, Y. Zhao, M. Lapsley, P. Li, J. P. McCoy, S. J. Levine and T. J. Huang, *Lab Chip*, 2014, **14**, 415–423.
64 X. Mao, A. A. Nawaz, S.-C. S. Lin, M. I. Lapsley, Y. Zhao, J. P. McCoy, W. S. El-Deiry and T. J. Huang, *Biomicrofluidics*, 2012, **6**, 024113.
65 Y. Chen, A. A. Nawaz, Y. Zhao, P.-H. Huang, J. P. McCoy, S. J. Levine, L. Wang and T. J. Huang, *Lab Chip*, 2014, **14**, 916–923.
66 C. Grenvall, C. Antfolk, C. Z. Bisgaard and T. Laurell, *Lab Chip*, 2014, **14**, 4629–4637.
67 A. Kalantarifard, A. Saateh and C. Elbuken, *Chemosensors*, 2018, **6**, 23.
68 H.-D. Xi, H. Zheng, W. Guo, A. M. Gañán-Calvo, Y. Ai, C.-W. Tsao, J. Zhou, W. Li, Y. Huang, N.-T. Nguyen and S. H. Tan, *Lab Chip*, 2017, **17**, 751–771.
69 S. L. Sjostrom, Y. Bai, M. Huang, Z. Liu, J. Nielsen, H. N. Joensson and H. Andersson Svahn, *Lab Chip*, 2014, **14**, 806–813.
70 R. H. Cole, S.-Y. Tang, C. A. Siltanen, P. Shahi, J. Q. Zhang, S. Poust, Z. J. Gartner and A. R. Abate, *Proc. Natl. Acad. Sci. U. S. A.*, 2017, **114**, 8728–8733.
71 C. Wu, X. Wei, X. Men, X. Zhang, Y.-L. Yu, Z.-R. Xu, M.-L. Chen and J.-H. Wang, *Anal. Chem.*, 2021, **93**(23), 8203–8209.
72 C. Wang, Y. Ma, Z. Chen, Y. Wu, F. Song, J. Qiu, M. Shi and X. Wu, *Cytometry, Part A*, 2021, **99**(10), 987–998.
73 Y.-J. Fan, Y.-C. Hsiao, Y.-L. Weng, Y.-H. Chen, P.-Y. Chiou and H.-J. Sheen, *Sens. Actuators, B*, 2020, **320**, 128255.
74 H. Pei, L. Li, Y. Wang, R. Sheng, Y. Wang, S. Xie, L. Shui, H. Si and B. Tang, *Anal. Chem.*, 2019, **91**, 11078–11084.
75 J. Wang, Z. Fan, Y. Zhao, Y. Song, H. Chu, W. Song, Y. Song, X. Pan, Y. Sun and D. Li, *Sci. Rep.*, 2016, **6**, 23165.
76 B. L. Fiedler, S. Van Buskirk, K. P. Carter, Y. Qin, M. C. Carpenter, A. E. Palmer and R. Jimenez, *Anal. Chem.*, 2017, **89**, 711–719.
77 X. Li, B. Fan, S. Cao, D. Chen, X. Zhao, D. Men, W. Yue, J. Wang and J. Chen, *Lab Chip*, 2017, **17**, 3129–3137.
78 T. Sato and R. Miyake, *Anal. Methods*, 2017, **9**, 3992–3997.
79 C. Kunstmann-Olsen, M. M. Hanczyc, J. Hoyland, S. Rasmussen and H.-G. Rubahn, *Sens. Actuators, B*, 2016, **229**, 7–13.
80 C.-S. Yan and Y.-N. Wang, *Biomed. Opt. Express*, 2016, **7**, 3585–3595.
81 Y. J. Heo, D. Lee, J. Kang, K. Lee and W. K. Chung, *Sci. Rep.*, 2017, **7**, 11651.
82 D. M. D. Siu, K. C. M. Lee, M. C. K. Lo, S. V. Stassen, M. Wang, I. Z. Q. Zhang, H. K. H. So, G. C. F. Chan, K. S. E. Cheah, K. K. Y. Wong, M. K. Y. Hsin, J. C. M. Ho and K. K. Tsia, *Lab Chip*, 2020, **20**, 3696–3708.
83 A. Isozaki, J. Harmon, Y. Zhou, S. Li, Y. Nakagawa, M. Hayashi, H. Mikami, C. Lei and K. Goda, *Lab Chip*, 2020, **20**, 3074–3090.
84 H. Mikami, M. Kawaguchi, C.-J. Huang, H. Matsumura, T. Sugimura, K. Huang, C. Lei, S. Ueno, T. Miura, T. Ito, K. Nagasawa, T. Maeno, H. Watarai, M. Yamagishi, S. Uemura, S. Ohnuki, Y. Ohya, H. Kurokawa, S. Matsusaka, C.-W. Sun, Y. Ozeki and K. Goda, *Nat. Commun.*, 2020, **11**, 1162.
85 A. Isozaki, H. Mikami, H. Tezuka, H. Matsumura, K. Huang, M. Akamine, K. Hiramatsu, T. Iino, T. Ito, H. Karakawa, Y. Kasai, Y. Li, Y. Nakagawa, S. Ohnuki, T. Ota, Y. Qian, S. Sakuma, T. Sekiya, Y. Shirasaki, N. Suzuki, E. Tayyabi, T. Wakamiya, M. Xu, M. Yamagishi, H. Yan, Q. Yu, S. Yan, D. Yuan, W. Zhang, Y. Zhao, F. Arai,

R. E. Campbell, C. Danelon, D. Di Carlo, K. Hiraki, Y. Hoshino, Y. Hosokawa, M. Inaba, A. Nakagawa, Y. Ohya, M. Oikawa, S. Uemura, Y. Ozeki, T. Sugimura, N. Nitta and K. Goda, *Lab Chip*, 2020, **20**, 2263–2273.

86 N. Nitta, T. Sugimura, A. Isozaki, H. Mikami, K. Hiraki, S. Sakuma, T. Iino, F. Arai, T. Endo, Y. Fujiwaki, H. Fukuzawa, M. Hase, T. Hayakawa, K. Hiramatsu, Y. Hoshino, M. Inaba, T. Ito, H. Karakawa, Y. Kasai, K. Koizumi, S. Lee, C. Lei, M. Li, T. Maeno, S. Matsusaka, D. Murakami, A. Nakagawa, Y. Oguchi, M. Oikawa, T. Ota, K. Shiba, H. Shintaku, Y. Shirasaki, K. Suga, Y. Suzuki, N. Suzuki, Y. Tanaka, H. Tezuka, C. Toyokawa, Y. Yalikun, M. Yamada, M. Yamagishi, T. Yamano, A. Yasumoto, Y. Yatomi, M. Yazawa, D. Di Carlo, Y. Hosokawa, S. Uemura, Y. Ozeki and K. Goda, *Cell*, 2018, **175**, 266–276.

87 Y. Han, R. Tang, Y. Gu, A. C. Zhang, W. Cai, V. Castor, S. H. Cho, W. Alaynick and Y.-H. Lo, *Optica*, 2019, **6**, 1297–1304.

88 Y. Gu, A. C. Zhang, Y. Han, J. Li, C. Chen and Y.-H. Lo, *Cytometry, Part A*, 2019, **95**, 499–509.

89 Y. Han, Y. Gu, A. C. Zhang and Y.-H. Lo, *Lab Chip*, 2016, **16**, 4639–4647.

90 M. Ossandon, J. Balsam, H. A. Bruck, K. Kalpakis and A. Rasooly, *Analyst*, 2017, **142**, 641–648.

91 S. Zhu, X. Zhang, Z. Zhou, Y. Han, N. Xiang and Z. Ni, *Talanta*, 2021, **233**, 122571.

92 Q. Zi, W. Ding, C. Sun, S. Li, D. Gao, L. He, J. Liu, L. Xu and B. Qiu, *Biosens. Bioelectron.*, 2020, **148**, 111820.

93 T. Tang, X. Liu, R. Kiya, Y. Shen, Y. Yuan, T. Zhang, K. Suzuki, Y. Tanaka, M. Li, Y. Hosokawa and Y. Yalikun, *Biosens. Bioelectron.*, 2021, **193**, 113521.

94 L. Gong, C. Petchakup, P. Shi, P. L. Tan, L. P. Tan, C. Y. Tay and H. W. Hou, *Small*, 2021, **17**, 2007500.

95 C. Petchakup, K. H. H. Li and H. W. Hou, *Micromachines*, 2017, **8**, 87.

96 J. Chen, C. Xue, Y. Zhao, D. Chen, M.-H. Wu and J. Wang, *Int. J. Mol. Sci.*, 2015, **16**, 9804–9830.

97 M. Serhatlioglu, M. Asghari, M. Tahsin Guler and C. Elbuken, *Electrophoresis*, 2019, **40**, 906–913.

98 Y. Feng, L. Huang, P. Zhao, F. Liang and W. Wang, *Anal. Chem.*, 2019, **91**, 15204–15212.

99 A. K. S. Lau, H. C. Shum, K. K. Y. Wong and K. K. Tsia, *Lab Chip*, 2016, **16**, 1743–1756.

100 M. Kumar, S. Yadav, A. Kumar, N. N. Sharma, J. Akhtar and K. Singh, *Biosens. Bioelectron.*, 2019, **142**, 111526.

101 S. Stavrakis, G. Holzner, J. Choo and A. deMello, *Curr. Opin. Biotechnol.*, 2019, **55**, 36–43.

102 P. Simon, M. Frankowski, N. Bock and J. Neukammer, *Lab Chip*, 2016, **16**, 2326–2338.

103 X. Liu, X. Huang, Y. Jiang, H. Xu, J. Guo, H. W. Hou, M. Yan and H. Yu, *IEEE Trans. Biomed. Circuits Syst.*, 2017, **11**, 794–803.

104 K. B. Roth, C. D. Eggleton, K. B. Neeves and D. W. M. Marr, *Lab Chip*, 2013, **13**, 1571–1577.

105 Z. Liu, Y. Lee, J. h. Jang, Y. Li, X. Han, K. Yokoi, M. Ferrari, L. Zhou and L. Qin, *Sci. Rep.*, 2015, **5**, 14272.

106 T. Sawetzki, C. D. Eggleton, S. A. Desai and D. W. M. Marr, *Biophys. J.*, 2013, **105**, 2281–2288.

107 J. Zhang, X. A. Nou, H. Kim and G. Scarcelli, *Lab Chip*, 2017, **17**, 663–670.

108 T. Blasi, H. Hennig, H. D. Summers, F. J. Theis, J. Cerveira, J. O. Patterson, D. Davies, A. Filby, A. E. Carpenter and P. Rees, *Nat. Commun.*, 2016, **7**, 10256.

109 K. Goda, A. Ayazi, D. R. Gossett, J. Sadasivam, C. K. Lonappan, E. Sollier, A. M. Fard, S. C. Hur, J. Adam, C. Murray, C. Wang, N. Brackbill, D. Di Carlo and B. Jalali, *Proc. Natl. Acad. Sci. U. S. A.*, 2012, **109**, 11630–11635.

110 Y. Jiang, C. Lei, A. Yasumoto, H. Kobayashi, Y. Aisaka, T. Ito, B. Guo, N. Nitta, N. Kutsuna, Y. Ozeki, A. Nakagawa, Y. Yatomi and K. Goda, *Lab Chip*, 2017, **17**, 2426–2434.

111 J. Zheng, T. Cole, Y. Zhang, J. Kim and S.-Y. Tang, *Biosens. Bioelectron.*, 2021, **194**, 113666.

112 A. Gupta, P. J. Harrison, H. Wieslander, N. Pielawski, K. Kartasalo, G. Partel, L. Solorzano, A. Suveer, A. H. Klemm, O. Spjuth, I.-M. Sintorn and C. Wählby, *Cytometry, Part A*, 2019, **95**, 366–380.

113 K. C. Cheung, M. Di Berardino, G. Schade-Kampmann, M. Hebeisen, A. Pierzchalski, J. Bocsi, A. Mittag and A. Tárnok, *Cytometry, Part A*, 2010, **77A**, 648–666.

114 F. Caselli and P. Bisegna, *Med. Eng. Phys.*, 2017, **48**, 81–89.

115 A. De Ninno, V. Errico, F. R. Bertani, L. Businaro, P. Bisegna and F. Caselli, *Lab Chip*, 2017, **17**, 1158–1166.

116 J. S. McGrath, C. Honrado, D. Spencer, B. Horton, H. L. Bridle and H. Morgan, *Sci. Rep.*, 2017, **7**, 2601.

117 Y. Zhao, X. T. Zhao, D. Y. Chen, Y. N. Luo, M. Jiang, C. Wei, R. Long, W. T. Yue, J. B. Wang and J. Chen, *Biosens. Bioelectron.*, 2014, **57**, 245–253.

118 C. Wyatt Shields Iv, C. D. Reyes and G. P. López, *Lab Chip*, 2015, **15**, 1230–1249.

119 A. Menachery, N. Kumawat and M. Qasaimeh, *TrAC, Trends Anal. Chem.*, 2017, **89**, 1–12.

120 C. Liu, *Cytometry, Part A*, 2018, **93**, 589–591.

121 A. Lenshof and T. Laurell, *Chem. Soc. Rev.*, 2010, **39**, 1203–1217.

122 A. Reece, B. Xia, Z. Jiang, B. Noren, R. McBride and J. Oakey, *Curr. Opin. Biotechnol.*, 2016, **40**, 90–96.

123 M. A. Witek, I. M. Freed and S. A. Soper, *Anal. Chem.*, 2020, **92**, 105–131.

124 Y. Shen, Y. Yalikun and Y. Tanaka, *Sens. Actuators, B*, 2019, **282**, 268–281.

125 Z. Cheng, X. Wu, J. Cheng and P. Liu, *Microfluid. Nanofluid.*, 2017, **21**, 9.

126 A. Isozaki, Y. Nakagawa, M. H. Loo, Y. Shibata, N. Tanaka, D. L. Setyaningrum, J.-W. Park, Y. Shirasaki, H. Mikami, D. Huang, H. Tsoi, C. T. Riche, T. Ota, H. Miwa, Y. Kanda, T. Ito, K. Yamada, O. Iwata, K. Suzuki, S. Ohnuki, Y. Ohya, Y. Kato, T. Hasunuma, S. Matsusaka, M. Yamagishi, M. Yazawa, S. Uemura, K. Nagasawa, H. Watarai, D. D. Carlo and K. Goda, *Sci. Adv.*, 2020, **6**, eaba6712.

127 D. J. Collins, A. Neild and Y. Ai, *Lab Chip*, 2016, **16**, 471–479.

128 S. Sakuma, Y. Kasai, T. Hayakawa and F. Arai, *Lab Chip*, 2017, **17**, 2760–2767.

129 B. de Wagenaar, S. Dekker, H. L. de Boer, J. G. Bomer, W. Olthuis, A. van den Berg and L. I. Segerink, *Lab Chip*, 2016, **16**, 1514–1522.
130 M. Huang, Y. Bai, S. L. Sjostrom, B. M. Hallström, Z. Liu, D. Petranovic, M. Uhlén, H. N. Joensson, H. Andersson-Svahn and J. Nielsen, *Proc. Natl. Acad. Sci. U. S. A.*, 2015, **112**, E4689–E4696.
131 B. E. Debs, R. Utharala, I. V. Balyasnikova, A. D. Griffiths and C. A. Merten, *Proc. Natl. Acad. Sci. U. S. A.*, 2012, **109**, 11570–11575.
132 T. Beneyton, F. Coldren, J.-C. Baret, A. D. Griffiths and V. Taly, *Analyst*, 2014, **139**, 3314–3323.
133 B. Watson, J. Friend and L. Yeo, *Sens. Actuators, A*, 2009, **152**, 219–233.
134 A. Barani, H. Paktinat, M. Janmaleki, A. Mohammadi, P. Mosaddegh, A. Fadaei-Tehrani and A. Sanati-Nezhad, *Biosens. Bioelectron.*, 2016, **85**, 714–725.
135 T. Jing, R. Ramji, M. E. Warkiani, J. Han, C. T. Lim and C.-H. Chen, *Biosens. Bioelectron.*, 2015, **66**, 19–23.
136 T. Jing, Z. Lai, L. Wu, J. Han, C. T. Lim and C.-H. Chen, *Anal. Chem.*, 2016, **88**, 11750–11757.
137 E. I. Galanzha and V. P. Zharov, *Cancers*, 2013, **5**, 1691–1738.
138 M. A. Juratli, M. Sarimollaoglu, E. R. Siegel, D. A. Nedosekin, E. I. Galanzha, J. Y. Suen and V. P. Zharov, *Head Neck*, 2014, **36**, 1207–1215.
139 B. Hamza, S. R. Ng, S. M. Prakadan, F. F. Delgado, C. R. Chin, E. M. King, L. F. Yang, S. M. Davidson, K. L. DeGouveia, N. Cermak, A. W. Navia, P. S. Winter, R. S. Drake, T. Tammela, C. M.-C. Li, T. Papagiannakopoulos, A. J. Gupta, J. Shaw Bagnall, S. M. Knudsen, M. G. Vander Heiden, S. C. Wasserman, T. Jacks, A. K. Shalek and S. R. Manalis, *Proc. Natl. Acad. Sci. U. S. A.*, 2019, **116**, 2232–2236.
140 S. Nagrath, L. V. Sequist, S. Maheswaran, D. W. Bell, D. Irimia, L. Ulkus, M. R. Smith, E. L. Kwak, S. Digumarthy, A. Muzikansky, P. Ryan, U. J. Balis, R. G. Tompkins, D. A. Haber and M. Toner, *Nature*, 2007, **450**, 1235–1239.
141 Q. Li, S. Cui, Y. Xu, Y. Wang, F. Jin, H. Si, L. Li and B. Tang, *Anal. Chem.*, 2019, **91**, 14133–14140.
142 J. S. McGrath, C. Honrado, J. H. Moore, S. J. Adair, W. B. Varhue, A. Salahi, V. Farmehini, B. J. Goudreau, S. Nagdas, E. M. Blais, T. W. Bauer and N. S. Swami, *Anal. Chim. Acta*, 2020, **1101**, 90–98.
143 A. Han, L. Yang and A. B. Frazier, *Clin. Cancer Res.*, 2007, **13**, 139–143.
144 A. Avram, C. Marculescu, C. M. Balan, C. Voitincu, C. Pirvulescu, M. Volmer, A. Popescu, M. Mihailescu and M. Avram, Microbiosensor for electrical impedance spectroscopic study of melanoma cells, CAS 2012 (International Semiconductor Conference), 2012, pp. 165–168.
145 G. Qiao, W. Duan, C. Chatwin, A. Sinclair and W. Wang, *J. Phys.: Conf. Ser.*, 2010, **224**, 012081.
146 O. Scheler, N. Pacocha, P. R. Debski, A. Ruszczak, T. S. Kaminski and P. Garstecki, *Lab Chip*, 2017, **17**, 1980–1987.
147 O. Scheler, T. S. Kaminski, A. Ruszczak and P. Garstecki, *ACS Appl. Mater. Interfaces*, 2016, **8**, 11318–11325.
148 J. Q. Boedicker, L. Li, T. R. Kline and R. F. Ismagilov, *Lab Chip*, 2008, **8**, 1265–1272.
149 W. A. Schell, J. L. Benton, P. B. Smith, M. Poore, J. L. Rouse, D. J. Boles, M. D. Johnson, B. D. Alexander, V. K. Pamula, A. E. Eckhardt, M. G. Pollack, D. K. Benjamin, J. R. Perfect and T. G. Mitchell, *Eur. J. Clin. Microbiol. Infect. Dis.*, 2012, **31**, 2237–2245.
150 C. L. Stoffel, R. F. Kathy and K. L. Rowlen, *Cytometry, Part A*, 2005, **65A**, 140–147.
151 J. Rho, W. Jang, I. Hwang, D. Lee, C. H. Lee and T. D. Chung, *Biosens. Bioelectron.*, 2018, **102**, 121–128.
152 S. Héritier, J.-F. Emile, M.-A. Barkaoui, C. Thomas, S. Fraitag, S. Boudjemaa, F. Renaud, A. Moreau, M. Peuchmaur, C. Chassagne-Clément, F. Dijoud, V. Rigau, D. Moshous, A. Lambilliotte, F. Mazingue, K. Kebaili, J. Miron, E. Jeziorski, G. Plat, N. Aladjidi, A. Ferster, H. Pacquement, C. Galambrun, L. Brugières, G. Leverger, L. Mansuy, C. Paillard, A. Deville, C. Armari-Alla, A. Lutun, M. Gillibert-Yvert, J.-L. Stephan, F. Cohen-Aubart, J. Haroche, I. Pellier, F. Millot, B. Lescoeur, V. Gandemer, C. Bodemer, R. Lacave, Z. Hélias-Rodzewicz, V. Taly, F. Geissmann and J. Donadieu, *J. Clin. Oncol.*, 2016, **34**, 3023–3030.
153 G. Zhu, X. Ye, Z. Dong, Y. C. Lu, Y. Sun, Y. Liu, R. McCormack, Y. Gu and X. Liu, *J. Mol. Diagn.*, 2015, **17**, 265–272.
154 E. Zonta, F. Garlan, N. Pécuchet, K. Perez-Toralla, O. Caen, C. Milbury, A. Didelot, E. Fabre, H. Blons, P. Laurent-Puig and V. Taly, *PLoS One*, 2016, **11**, e0159094.
155 M. Watanabe, T. Kawaguchi, S.-i. Isa, M. Ando, A. Tamiya, A. Kubo, H. Saka, S. Takeo, H. Adachi, T. Tagawa, S. Kakegawa, M. Yamashita, K. Kataoka, Y. Ichinose, Y. Takeuchi, K. Sakamoto, A. Matsumura and Y. Koh, *Clin. Cancer Res*, 2015, **21**, 3552.
156 T. Takahama, K. Sakai, M. Takeda, K. Azuma, T. Hida, M. Hirabayashi, T. Oguri, H. Tanaka, N. Ebi, T. Sawa, A. Bessho, M. Tachihara, H. Akamatsu, S. Bandoh, D. Himeji, T. Ohira, M. Shimokawa, Y. Nakanishi, K. Nakagawa and K. Nishio, *Oncotarget*, 2016, **7**(36), 58492–58499.
157 M. F. Sanmamed, S. Fernández-Landázuri, C. Rodríguez, R. Zárate, M. D. Lozano, L. Zubiri, J. L. Perez-Gracia, S. Martín-Algarra and A. González, *Clin. Chem.*, 2015, **61**, 297–304.
158 A. G. Sacher, C. Paweletz, S. E. Dahlberg, R. S. Alden, A. O'Connell, N. Feeney, S. L. Mach, P. A. Jänne and G. R. Oxnard, *JAMA Oncol.*, 2016, **2**, 1014–1022.
159 A. L. Reid, J. B. Freeman, M. Millward, M. Ziman and E. S. Gray, *Clin. Biochem.*, 2015, **48**, 999–1002.
160 G. R. Oxnard, C. P. Paweletz, Y. Kuang, S. L. Mach, A. Connell, M. M. Messineo, J. J. Luke, M. Butaney, P. Kirschmeier, D. M. Jackman and P. A. Jänne, *Clin. Cancer Res.*, 2014, **20**, 1698.

161 B. J. Hindson, K. D. Ness, D. A. Masquelier, P. Belgrader, N. J. Heredia, A. J. Makarewicz, I. J. Bright, M. Y. Lucero, A. L. Hiddessen, T. C. Legler, T. K. Kitano, M. R. Hodel, J. F. Petersen, P. W. Wyatt, E. R. Steenblock, P. H. Shah, L. J. Bousse, C. B. Troup, J. C. Mellen, D. K. Wittmann, N. G. Erndt, T. H. Cauley, R. T. Koehler, A. P. So, S. Dube, K. A. Rose, L. Montesclaros, S. Wang, D. P. Stumbo, S. P. Hodges, S. Romine, F. P. Milanovich, H. E. White, J. F. Regan, G. A. Karlin-Neumann, C. M. Hindson, S. Saxonov and B. W. Colston, *Anal. Chem.*, 2011, **83**, 8604–8610.

162 K. Otsuji, T. Sasaki, A. Tanaka, A. Kunita, M. Ikemura, K. Matsusaka, K. Tada, M. Fukayama and Y. Seto, *Breast Cancer Res. Treat.*, 2017, **162**, 11–18.

163 H. Kinugasa, K. Nouso, T. Tanaka, K. Miyahara, Y. Morimoto, C. Dohi, T. Matsubara, H. Okada and K. Yamamoto, *Br. J. Cancer*, 2015, **112**, 1652–1655.

164 N. J. Heredia, P. Belgrader, S. Wang, R. Koehler, J. Regan, A. M. Cosman, S. Saxonov, B. Hindson, S. C. Tanner, A. S. Brown and G. Karlin-Neumann, *Methods*, 2013, **59**, S20–S23.

165 P. Belgrader, S. C. Tanner, J. F. Regan, R. Koehler, B. J. Hindson and A. S. Brown, *Clin. Chem.*, 2013, **59**, 991–994.

166 Q. Zhong, S. Bhattacharya, S. Kotsopoulos, J. Olson, V. Taly, A. D. Griffiths, D. R. Link and J. W. Larson, *Lab Chip*, 2011, **11**, 2167–2174.

167 V. Taly, D. Pekin, L. Benhaim, S. K. Kotsopoulos, D. Le Corre, X. Li, I. Atochin, D. R. Link, A. D. Griffiths, K. Pallier, H. Blons, O. Bouché, B. Landi, J. B. Hutchison and P. Laurent-Puig, *Clin. Chem.*, 2013, **59**, 1722–1731.

168 D. Pekin and V. Taly, in *Microchip Diagnostics: Methods and Protocols*, ed. V. Taly, J.-L. Viovy and S. Descroix, Springer New York, New York, NY, 2017, pp. 143–164, DOI: **10.1007/978-1-4939-6734-6_12**.

169 P. Laurent-Puig, D. Pekin, C. Normand, S. K. Kotsopoulos, P. Nizard, K. Perez-Toralla, R. Rowell, J. Olson, P. Srinivasan, D. Le Corre, T. Hor, Z. El Harrak, X. Li, D. R. Link, O. Bouché, J.-F. Emile, B. Landi, V. Boige, J. B. Hutchison and V. Taly, *Clin. Cancer Res.*, 2015, **21**, 1087.

170 M. M. Kiss, L. Ortoleva-Donnelly, N. R. Beer, J. Warner, C. G. Bailey, B. W. Colston, J. M. Rothberg, D. R. Link and J. H. Leamon, *Anal. Chem.*, 2008, **80**, 8975–8981.

171 G. S. Brunetto, R. Massoud, E. C. Leibovitch, B. Caruso, K. Johnson, J. Ohayon, K. Fenton, I. Cortese and S. Jacobson, *J. NeuroVirol.*, 2014, **20**, 341–351.

172 J. Pavšič, J. Žel and M. Milavec, *Anal. Bioanal. Chem.*, 2016, **408**, 67–75.

173 J.-T. Huang, Y.-J. Liu, J. Wang, Z.-G. Xu, Y. Yang, F. Shen, X.-h. Liu, X. Zhou and S.-M. Liu, *Clin. Chem.*, 2015, **61**, 290–296.

174 M. C. Strain, S. M. Lada, T. Luong, S. E. Rought, S. Gianella, V. H. Terry, C. A. Spina, C. H. Woelk and D. D. Richman, *PLoS One*, 2013, **8**, e55943.

175 K. Kelley, A. Cosman, P. Belgrader, B. Chapman and D. C. Sullivan, *J. Clin. Microbiol.*, 2013, **51**, 2033–2039.

176 J. Luo, J. Li, H. Yang, J. Yu, H. Wei and N. A. Ledeboer, *J. Clin. Microbiol.*, 2017, **55**, 2946–2955.

177 N. R. Beer, E. K. Wheeler, L. Lee-Houghton, N. Watkins, S. Nasarabadi, N. Hebert, P. Leung, D. W. Arnold, C. G. Bailey and B. W. Colston, *Anal. Chem.*, 2008, **80**, 1854–1858.

178 M. Mukaide, M. Sugiyama, M. Korenaga, K. Murata, T. Kanto, N. Masaki and M. Mizokami, *J. Virol. Methods*, 2014, **207**, 169–177.

179 M. Kiselinova, A. O. Pasternak, W. De Spiegelaere, D. Vogelaers, B. Berkhout and L. Vandekerckhove, *PLoS One*, 2014, **9**, e85999.

180 W. Guan, L. Chen, T. D. Rane and T.-H. Wang, *Sci. Rep.*, 2015, **5**, 13795.

181 Y. Hu, P. Xu, J. Luo, H. He and W. Du, *Anal. Chem.*, 2017, **89**, 745–750.

182 J.-u. Shim, R. T. Ranasinghe, C. A. Smith, S. M. Ibrahim, F. Hollfelder, W. T. S. Huck, D. Klenerman and C. Abell, *ACS Nano*, 2013, **7**, 5955–5964.

183 H. N. Joensson, M. L. Samuels, E. R. Brouzes, M. Medkova, M. Uhlén, D. R. Link and H. Andersson-Svahn, *Angew. Chem., Int. Ed.*, 2009, **48**, 2518–2521.

184 E. X. Ng, M. A. Miller, T. Jing, D. A. Lauffenburger and C.-H. Chen, *Lab Chip*, 2015, **15**, 1153–1159.

185 C.-H. Chen, M. A. Miller, A. Sarkar, M. T. Beste, K. B. Isaacson, D. A. Lauffenburger, L. G. Griffith and J. Han, *J. Am. Chem. Soc.*, 2013, **135**, 1645–1648.

186 C.-H. Chen, A. Sarkar, Y.-A. Song, M. A. Miller, S. J. Kim, L. G. Griffith, D. A. Lauffenburger and J. Han, *J. Am. Chem. Soc.*, 2011, **133**, 10368–10371.

187 T. D. Rane, H. C. Zec and T.-H. Wang, *Anal. Chem.*, 2015, **87**, 1950–1956.

188 S. Jambovane, D. J. Kim, E. C. Duin, S.-K. Kim and J. W. Hong, *Anal. Chem.*, 2011, **83**, 3358–3364.

189 J. Lim, J. Vrignon, P. Gruner, C. S. Karamitros, M. Konrad and J.-C. Baret, *Appl. Phys. Lett.*, 2013, **103**, 203704.

190 Z. Li, A. M. Leshansky, L. M. Pismen and P. Tabeling, *Lab Chip*, 2015, **15**, 1023–1031.

191 M. Najah, E. Mayot, I. P. Mahendra-Wijaya, A. D. Griffiths, S. Ladame and A. Drevelle, *Anal. Chem.*, 2013, **85**, 9807–9814.

192 S. Gu, Y. Lu, Y. Ding, L. Li, H. Song, J. Wang and Q. Wu, *Biosens. Bioelectron.*, 2014, **55**, 106–112.

193 M. Y. H. Tang and H. C. Shum, *Lab Chip*, 2016, **16**, 4359–4365.

194 Z. Han, W. Li, Y. Huang and B. Zheng, *Anal. Chem.*, 2009, **81**, 5840–5845.

195 R. Arayanarakool, L. Shui, S. W. M. Kengen, A. van den Berg and J. C. T. Eijkel, *Lab Chip*, 2013, **13**, 1955–1962.

196 F. Fachin, P. Spuhler, J. M. Martel-Foley, J. F. Edd, T. A. Barber, J. Walsh, M. Karabacak, V. Pai, M. Yu, K. Smith, H. Hwang, J. Yang, S. Shah, R. Yarmush, L. V. Sequist, S. L. Stott, S. Maheswaran, D. A. Haber, R. Kapur and M. Toner, *Sci. Rep.*, 2017, **7**, 10936.

197 L. Zhao, C. Tang, L. Xu, Z. Zhang, X. Li, H. Hu, S. Cheng, W. Zhou, M. Huang, A. Fong, B. Liu, H.-R. Tseng, H. Gao, Y. Liu and X. Fang, *Small*, 2016, **12**, 1072–1081.
198 W. Sheng, T. Chen, R. Kamath, X. Xiong, W. Tan and Z. H. Fan, *Anal. Chem.*, 2012, **84**, 4199–4206.
199 P. Li, Z. Mao, Z. Peng, L. Zhou, Y. Chen, P.-H. Huang, C. I. Truica, J. J. Drabick, W. S. El-Deiry, M. Dao, S. Suresh and T. J. Huang, *Proc. Natl. Acad. Sci. U. S. A.*, 2015, **112**, 4970–4975.
200 E. S. Park, C. Jin, Q. Guo, R. R. Ang, S. P. Duffy, K. Matthews, A. Azad, H. Abdi, T. Todenhöfer, J. Bazov, K. N. Chi, P. C. Black and H. Ma, *Small*, 2016, **12**, 1909–1919.
201 M. E. Warkiani, G. Guan, K. B. Luan, W. C. Lee, A. A. S. Bhagat, P. Kant Chaudhuri, D. S.-W. Tan, W. T. Lim, S. C. Lee, P. C. Y. Chen, C. T. Lim and J. Han, *Lab Chip*, 2014, **14**, 128–137.
202 E. Sollier, D. E. Go, J. Che, D. R. Gossett, S. O'Byrne, W. M. Weaver, N. Kummer, M. Rettig, J. Goldman, N. Nickols, S. McCloskey, R. P. Kulkarni and D. Di Carlo, *Lab Chip*, 2014, **14**, 63–77.
203 S. H. Au, J. Edd, A. E. Stoddard, K. H. K. Wong, F. Fachin, S. Maheswaran, D. A. Haber, S. L. Stott, R. Kapur and M. Toner, *Sci. Rep.*, 2017, **7**, 2433.
204 A. F. Sarioglu, N. Aceto, N. Kojic, M. C. Donaldson, M. Zeinali, B. Hamza, A. Engstrom, H. Zhu, T. K. Sundaresan, D. T. Miyamoto, X. Luo, A. Bardia, B. S. Wittner, S. Ramaswamy, T. Shioda, D. T. Ting, S. L. Stott, R. Kapur, S. Maheswaran, D. A. Haber and M. Toner, *Nat. Methods*, 2015, **12**, 685–691.
205 M. Avram, C. M. Bălan, I. Petrescu, V. Schiopu, C. Mărculescu and A. Avram, *Plasmonics*, 2012, **7**, 717–724.
206 S. Faez, Y. Lahini, S. Weidlich, R. F. Garmann, K. Wondraczek, M. Zeisberger, M. A. Schmidt, M. Orrit and V. N. Manoharan, *ACS Nano*, 2015, **9**, 12349–12357.
207 T. D. Rane, H. C. Zec, C. Puleo, A. P. Lee and T.-H. Wang, *Lab Chip*, 2012, **12**, 3341–3347.
208 D.-K. Kang, M. M. Ali, K. Zhang, S. S. Huang, E. Peterson, M. A. Digman, E. Gratton and W. Zhao, *Nat. Commun.*, 2014, **5**, 5427.
209 D. Pekin, Y. Skhiri, J.-C. Baret, D. Le Corre, L. Mazutis, C. Ben Salem, F. Millot, A. El Harrak, J. B. Hutchison, J. W. Larson, D. R. Link, P. Laurent-Puig, A. D. Griffiths and V. Taly, *Lab Chip*, 2011, **11**, 2156–2166.
210 S. Mader and K. Pantel, *Oncol. Res. Treat.*, 2017, **40**, 404–408.
211 H. Schwarzenbach, D. S. B. Hoon and K. Pantel, *Nat. Rev. Cancer*, 2011, **11**, 426–437.
212 D. J. Shin, Y. Zhang and T.-H. Wang, *Microfluid. Nanofluid.*, 2014, **17**, 425–430.
213 Y. Zhang, S. Park, S. Yang and T.-H. Wang, *Biomed. Microdevices*, 2010, **12**, 1043–1049.
214 Q. Wu, W. Jin, C. Zhou, S. Han, W. Yang, Q. Zhu, Q. Jin and Y. Mu, *Anal. Chem.*, 2011, **83**, 3336–3342.
215 N. Rački, D. Morisset, I. Gutierrez-Aguirre and M. Ravnikar, *Anal. Bioanal. Chem.*, 2014, **406**, 661–667.
216 S. M. Hanash, C. S. Baik and O. Kallioniemi, *Nat. Rev. Clin. Oncol.*, 2011, **8**, 142–150.